

# 1 **Optimal planning of natural stormwater solutions** 2 **using a composite Gini coefficient: A watershed** 3 **assessment of hydrological, environmental, social,** 4 **and economic efficiency** 5

6 Cyndi V. Castro <sup>a,\*</sup>

7 <sup>a</sup>*Department of Civil Engineering, University of Illinois at Urbana-Champaign, Urbana, IL,*  
8 *61801, USA*

## 9 **Abstract**

10 A robust multi-functional framework for widespread planning of nature-based solutions (NBS)  
11 must incorporate components of social equity and hydro-environmental performance in a cost-  
12 effective manner. NBS systems address stormwater mitigation by increasing on-site infiltration  
13 and evaporation through enhanced greenspace while also improving various components of  
14 societal well-being, such as physical health (e.g., heart disease, diabetes), mental health (e.g., post-  
15 traumatic stress disorder, depression), and sense of place. However, current optimization tools for  
16 NBS systems rely on stormwater quantity abatement and, to a lesser extent, economic costs and  
17 environmental pollutant mitigation. Therefore, the objective of this study is to explore how NBS  
18 planning may be improved to maximize hydrological, environmental, and social co-benefits in an  
19 unequivocal and equitable manner. Here, a large-scale NBS watershed was calibrated to local  
20 conditions using standard hydro-environmental modeling and optimized according to the  
21 traditional NBS planning paradigm (i.e., on the basis of stormwater abatement, pollutant load  
22 reduction, and economic efficacy). The resulting NBS allocation was then integrated with spatial  
23 properties of social deprivation through a novel framework involving the Area Deprivation Index  
24 (ADI) and a multi-functional Gini coefficient. This framework allows us to better understand and  
25 optimize how social, environmental, and hydrological impacts differ across human populations

26 and landscapes as a function of cost. By embedding social equity as an explicit optimization  
27 objective within the fabric of the NBS planning process, this study provides a strategic opportunity  
28 for addressing social justice and spurring community buy-in toward balanced NBS systems.

## 29 **Highlights**

- 30 1. Nature-based solutions (NBSs) are traditionally planned to maximize stormwater  
31 abatement potential while minimizing implementation costs.
- 32 2. Research has demonstrated the capability of NBSs to address issues of societal well-  
33 being, such as improved mental and physical health.
- 34 3. A novel framework is proposed and demonstrated to combine hydro-environmental  
35 modeling with social deprivation using the Gini coefficient.

## 36 *Keywords:*

- 37 → area deprivation index (ADI)
- 38 → Gini coefficient
- 39 → low impact development
- 40 → multi-objective optimization
- 41 → storm water management model (SWMM)
- 42 → social equity

## 43 **1 Introduction**

44 Nature-based solutions (NBSs) are expected to become a central tool for climate change  
45 adaptation, and we necessitate enhanced approaches to synchronize resiliency goals associated  
46 with societal well-being, environmental justice, and natural hazard mitigation. NBSs describe a  
47 collection of sustainable management approaches that emulate natural processes to address hydro-  
48 environmental hazards while simultaneously providing social and ecosystem benefits. NBSs have  
49 evolved within the literature to encompass the urban drainage concepts of green infrastructure  
50 (GI), low-impact development (LID), best management practices (BMPs), sustainable urban  
51 drainage systems (SuDs), water-sensitive urban design (WSUD), and blue-green infrastructure  
52 (BGI) (Ruangpan et al., 2020). As such, the predominant modeling schemes used for NBS  
53 planning have typically highlighted hydrological efficacy with less attention to social  
54 characteristics (Zhang and Chui, 2018). However, we know that the location of human settlements  
55 can influence several social factors that have been linked to NBS co-benefits, such as  
56 improvements in communal well-being, mental health, recreation, and physical health (Alves et  
57 al., 2019; Fenner, 2017; Li et al., 2017). By providing enhanced greenspaces and social gathering  
58 places, NBSs have been linked to a reduction in cardiovascular disease, diabetes, cancer, mental  
59 disorders, and chronic respiratory diseases, which are disproportionately higher among racial and  
60 ethnic minorities and the socioeconomically disadvantaged (Astell-Burt and Feng, 2021; Brown  
61 et al., 2016; Fuertes et al., 2014; Gascon et al., 2016; Maas et al., 2009; Mitchell and Popham,  
62 2008; Ray and Jakubec, 2014). As such, we must integrate hydro-environmental and social  
63 characteristics to realize the full benefits of NBSs.

64 At the local scale (i.e., laboratory-, plot-, neighborhood-scale), NBS technologies have shown  
65 great promise in addressing both stormwater abatement goals and socio-environmental co-benefits

66 (Jato-Espino et al., 2016; Kabisch et al., 2016; Loperfido et al., 2014). At the regional scale,  
67 however, widespread use of NBS technologies has been limited due to a lack of understanding the  
68 complex interactions between physical characteristics and social conditions (Lim and Welty, 2017;  
69 Zhang and Chui, 2018). When planning for NBS systems, there will exist inherent tradeoffs  
70 between spatial priority and functionality that must be considered. The optimal spatial  
71 configuration of an NBS system is a function of overlapping rainfall patterns, watershed properties,  
72 equity factors, environmental triggers, ecological considerations, socio-demographics, risk and  
73 vulnerability, and other underlying principles that have not been fully elucidated (Perez-Pedini et  
74 al., 2005). Traditionally, NBS optimization schemes have continued to prioritize drainage  
75 characteristics in lieu of social functionality throughout space, while assuming such co-benefits  
76 will somehow propagate naturally throughout the system (Ruangpan et al., 2020; Zhang and Chui,  
77 2018). In this way, NBS multi-functionalities are not included as an explicit representation of their  
78 full locational benefits, thus limiting the maximum potential of NBSs to mitigate cross-cutting  
79 issues within the urban fabric. A right first step toward fully encompassing NBS multi-  
80 functionalities is to represent disparate phenomena as functions of space and to quantify their  
81 tradeoffs through the lens of multiple, overlapping disciplines.

82 In the age of the Anthropocene, where hydrologic, environmental, and social processes are  
83 being influenced and altered by human patterns, we are starting to study Earth systems outside of  
84 the traditionally-fixed vacuum of ideal physical boundary conditions. Researchers are beginning  
85 to couple biophysical processes with societal influences through the flourishing fields of socio-  
86 hydrology, coupled human and natural systems (CHANS), socio-ecology, and others (Blair and  
87 Buytaert, 2016). The hydrological community is suggesting that we address socio-environmental  
88 justices by integrating transdisciplinary variables into watershed modeling frameworks. Much of

89 the recent progress in socio-hydrology has evolved from a combination of exploratory frameworks  
90 (i.e. feedbacks, causal relationships, patterns) with water balance models and system dynamics  
91 (Kuil et al., 2016; Pande and Sivapalan, 2017). While such couplings have been widely noted  
92 within the literature, they are seldom quantitated and considered holistically in NBS management  
93 frameworks (Ruangpan et al., 2020).

94 NBS systems are instead typically planned with either simplified data-overlay methods for  
95 defining hot-spots of vulnerable locations or complex hydro-dynamic programs that prioritize  
96 stormwater volume abatement over social functionalities (Madureira and Andresen, 2014; Zhang  
97 and Chui, 2018), with the latter being limited in their scale of analysis due to large data  
98 requirements and computational difficulties (Barco et al., 2009). By relying on complex modeling  
99 tools (i.e., SWMM, MIKE-URBAN), most NBS studies have tended to neglect the social  
100 dimension altogether in favor of earth-system processes, thereby lacking optimal configurations  
101 for capturing holistic co-benefits (Kandakoglu et al., 2019). For these reasons, widespread  
102 adoption of green infrastructure has generally remained stunted, despite the ongoing evidence that  
103 NBSs provide efficient stormwater mitigation, lower costs in comparison to traditional grey  
104 infrastructure, and numerous social benefits (Golden and Hoghooghi, 2018; Madureira and  
105 Andresen, 2014). A recent state-of-the-art review described how consideration of multiple co-  
106 benefits has been increasingly valued as a desirable goal throughout the NBS literature, yet the  
107 majority of NBS planning has continued to prioritize stormwater abatement, due in part to a lack  
108 of integrated socio-hydrological frameworks (Ruangpan et al., 2020). We thereby have substantial  
109 knowledge gaps regarding informed NBS optimization (Golden and Hoghooghi, 2018; Kabisch et  
110 al., 2016), as interactions between NBS phenomena and the social conditions with which they aim  
111 to address are poorly represented in our existing frameworks (Lim and Welty, 2017). As such,

112 explicit representation of the social co-benefits of NBS systems is one of the most critical barriers  
113 to overcome for widespread success in this field (Adib and Wu, 2020).

114

115 In addition to a lack of robust representation of social characteristics within NBS optimization  
116 frameworks, the decision to implement NBS within a given locale is also highly dependent on  
117 stakeholder buy-in (Van de Meene et al., 2011; Wihlborg et al., 2019). NBSs are unlike traditional  
118 stormwater infrastructure due to regular human interaction with the greenspaces, which impacts  
119 social well-being. Many NBS technologies, such as roof gardens or rainwater harvesting systems,  
120 function as an optimal unit when implementation occurs on both public and private properties. In  
121 this respect, local community buy-in is essential for achieving widespread NBS adoption. Studies  
122 have demonstrated how NBS implementation continues to be limited due to the inability for  
123 decision-makers to visualize overlapping co-benefits at the local scale (Adib and Wu, 2020; Liu  
124 and Jensen, 2018; Sarabi et al., 2019; Van de Meene et al., 2011; Wamsler et al., 2020; Wihlborg  
125 et al., 2019). Studies have also shown that attitudes regarding NBSs are improved when  
126 stakeholders can readily identify how NBS solutions will benefit their locale in a manner that  
127 extends beyond stormwater performance (Liu and Jensen, 2018; Sarabi et al., 2020; Wamsler et  
128 al., 2020). In other words, robust NBS implementation will not occur until city planners are able  
129 to identify and prioritize the multiple co-benefits involved in the NBS system. As such, in order to  
130 fully capture the multi-functionalities of NBS systems and improve implementation, we  
131 necessitate innovative optimization frameworks encompassing the variety of physical and social  
132 functionalities associated with NBSs.

133 Current stormwater management within the study area (Houston, Texas, USA) is based on a  
134 ‘worst-first’ framework (Despart, 2019), where hydrological improvements are prioritized

135 according to flood risk reduction and the number of persons benefited, irrespective of their socio-  
136 economic conditions. Such frameworks do not address inherent vulnerabilities within the  
137 populations served to consider human aspects, such as ability to recover from a storm or the  
138 reinforcing impacts of hydro-environmental hazards on socio-economics. This study re-shapes the  
139 NBS planning process by transcending beyond flood risk to also include components of social  
140 characteristics as a policy-making mechanism. Here, a novel equity-based indexing framework is  
141 proposed to better understand how we might optimize social and physical functionalities of NBS  
142 systems as a function of trans-disciplinary characteristics. Specifically, we explore the spatial  
143 tradeoffs associated with NBS allocation by first optimizing a local watershed-scale model  
144 according to traditional metrics of efficacy (e.g., cost efficiency, hydrological runoff reduction,  
145 and pollutant load reduction). We then identify the statistical dispersion of social vulnerability  
146 using the Area Deprivation Index (ADI), which is a spatial account of neighborhood disadvantage  
147 according to United States census characteristics. The ADI is incorporated into the optimization  
148 scheme using a novel area Gini coefficient and Lorenz curve. This framework is intended to spur  
149 the positive connection of social and physical influences within robust NBS planning.

## 150 **2 Materials and Methods**

### 151 *2.1 Area Deprivation Index*

152 The ADI was introduced in 2016 as a proxy indicator of socio-economic status from census  
153 results that have been curated to reflect the highest risk factors associated with long-term health  
154 (Knighton et al., 2016). The ADI is primarily used within the medical literature to measure social  
155 determinants that have been shown to influence public health issues, such as cancer rates (Kurani  
156 et al., 2020), hospital admissions (Hirshberg et al., 2019; Ingraham et al., 2021), asthma (Nkoy et  
157 al., 2018), obesity (Ludwig et al., 2011), diabetes (Addala et al., 2021), mental health (Martikainen

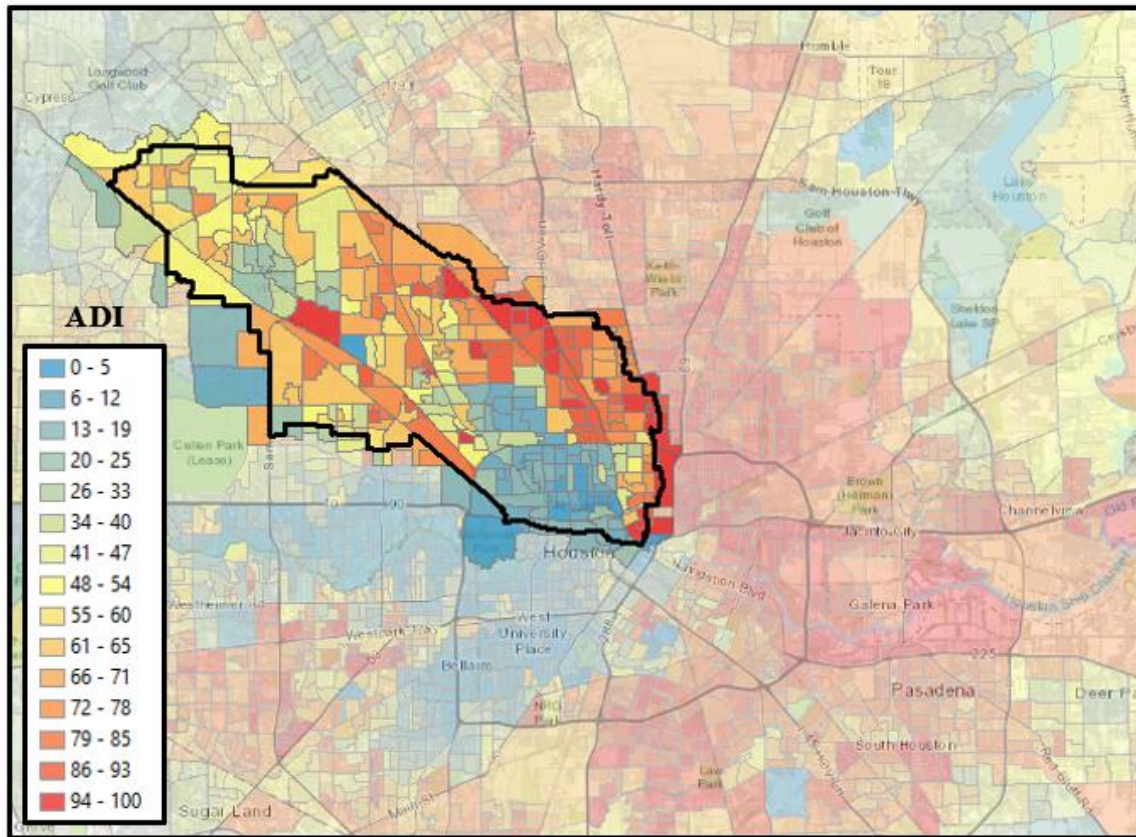
158 et al., 2004), and mortality (Chamberlain et al., 2020; Singh, 2003), each of which are impacted  
159 by NBS systems (van den Bosch and Ode Sang, 2017). The ADI merges characteristics of income,  
160 employment, education, and housing from the United States census to represent social  
161 disadvantage (Kind and Buckingham, 2018), which have been shown collectively to influence  
162 communal health (Link and Phelan, 1995).

163 An advantage of using the ADI for NBS planning, as opposed to other social indices, involves  
164 its highly-granular geospatial scale. The ADI provides a unique measurement of social deprivation  
165 for each census block group within the United States. Other standard metrics of social  
166 vulnerability, such as the Center for Disease Control (CDC) Social Vulnerability Index (SVI)  
167 (Flanagan et al., 2020), are delineated at the census tract-scale, thereby lacking spatial  
168 heterogeneity to assess key differences at the local-scale. [Note: Census tracts are subdivisions of  
169 counties encompassing approximately 4,000 residents within each bound. Block groups are  
170 subdivisions of census tracts encompassing approximately 250-550 housing units, demarcated by  
171 local streets (Schlossberg, 2003).]

172 The ADI for the study area was downloaded from the University of Wisconsin's Neighborhood  
173 Atlas for year 2019 (Kind and Buckingham, 2018). The weighted ADI values within each spatial  
174 unit are represented at the national-level by a percentile (1-100) and at the state-level by a decile  
175 (1-10), with lower values denoting greater disadvantage (University of Wisconsin School of  
176 Medicine and Public, 2019). For example, an ADI value of 1 on the national-scale represents an  
177 area that is more disadvantaged than the remaining 99% of census blocks within the nation. At the  
178 state-scale, an ADI of 1 implies that the given census block is more disadvantaged than 90% of  
179 the other census blocks within that state.



180 Here, the national-level ADI was used to depict spatial variation of social inequity throughout  
181 the White Oak Bayou (WOB) watershed in Houston, Texas, USA. The WOB watershed was  
182 chosen for this case study as it contains a highly-heterogeneous representation of socio-economic  
183 status, as represented in **Fig. 1**.



184  
185 **Fig. 1.** Area deprivation index for the White Oak Bayou watershed.

186 *2.2 Hydro-environmental SWMM Model*

187 *2.2.1 Hydrological Modeling*

188 The basin model for the WOB watershed was initialized using the HMS-PrePro tool, which  
189 rapidly delineates a watershed into subcatchments according to the local terrain, connects  
190 hydrological topology in a format consistent with standard hydrological modeling software, and  
191 estimates common hydrological parameters to represent basin infiltration, runoff, and channelized

192 routing of flow (Castro and Maidment, 2020). The Green-Ampt method was used to represent  
193 infiltration losses within each subcatchment according to local empirical values used in FEMA-  
194 effective hydrology models for the WOB watershed (HCFCD, 2019) (initial content = 0.067,  
195 saturated content = 0.46, suction = 3.553 inches, conductivity = 0.032 inches/hour). The SWMM  
196 software routes overland flow to the subcatchment outlet using a property called the ‘characteristic  
197 width’, which is defined as the subcatchment area divided by the average maximum overland flow  
198 length (Rossman and Huber, 2016). The longest flow path for each subcatchment was calculated  
199 in HMS-PrePro according to 2018 LiDAR at 10-centimeter resolution (TNRIS, 2019). The time  
200 of concentration for each subcatchment was calculated using the TR-55 methodology for urban  
201 watersheds (USDA, 1986). Other principal inputs for modeling subcatchments in SWMM include  
202 average land use, impervious coverage, subcatchment area, and terrain slope, which were each  
203 estimated using HMS-PrePro.

204 PCSWMM version 7.4.3240 (Hamouz et al., 2020), which is a proprietary software designed  
205 as a user-friendly interface to the Environmental Protection Agency (EPA) SWMM program, was  
206 used to convert the preliminary basin into a SWMM model. To route flow through the watershed  
207 stream network, the PCSWMM Transect Tool was used to create average cross-sections for each  
208 system channel from the 2018 LiDAR elevation model (CHI, 2014). Design storm data for the  
209 Houston region was obtained from Barrett (2019) and COH (2019) to represent the latest Atlas  
210 14 precipitation frequency estimates in Texas, according to the National Oceanic and Atmospheric  
211 Administration (NOAA) (Perica et al., 2018). The rainfall intensity values for the Houston-area  
212 were used to develop intensity-duration-frequency (IDF) curves in PCSWMM for varying annual  
213 exceedance probability (AEP) storm events (summarized in **Table S.1**). The IDF curve estimates

214 a frequency of occurrence for extreme precipitation events, which is commonly used to design  
215 urban stormwater infrastructure (Koutsoyiannis et al., 1998).

### 216 2.2.2 *Pollutant Load Modeling*

217 The event mean concentration (EMC) method was used to estimate non-point water pollution  
218 within each subcatchment according to

$$219 \quad EMC_s = \frac{\int C_s Q_s dt}{\int Q_s dt}, \quad (1)$$

220 where  $EMC_s$  is the event mean concentration,  $C_s$  is the standard concentration of a target pollutant,  
221 and  $Q_s$  is the runoff volume for each subcatchment,  $s$ , changing over simulation time  $t$ .

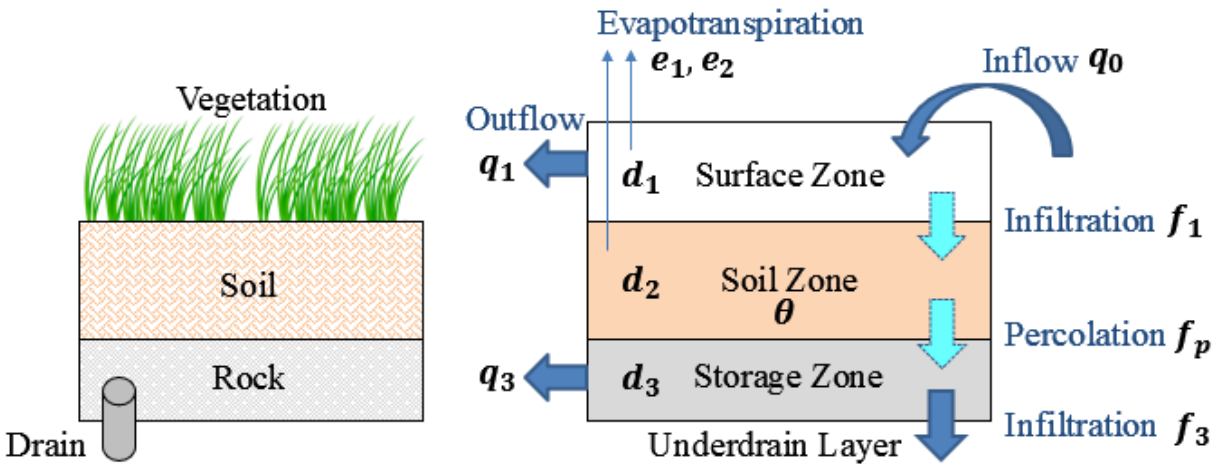
222 Local stormwater monitoring data was obtained from the National Stormwater Quality  
223 Database (NSQD), which contains public water quality meta-data from over 9,000 runoff events  
224 for approximately 200 municipalities in the United States, including 41 monitoring stations within  
225 Harris County, Texas (Pitt et al., 2015). Since the GreenPlan-IT algorithm searches for the most  
226 cost-effective solution according to an individual pollutant type (further described in **Section 0**),  
227 total suspended solids (TSS) were chosen as the criteria pollutant due to the strong adsorption  
228 effects of TSS on other contaminants (Liu et al., 2019; Rossi et al., 2006). Pooled values of TSS  
229 concentrations were obtained for each land use type within the NSQD, as summarized in **Table**  
230 **S.2**. In watershed-scale modeling, pooled load concentrations are common and have not been  
231 shown to pose a significant impact on the resulting model outcomes, particularly when the purpose  
232 of analysis is for comparison between scenarios (Lin, 2004; White et al., 2015).

233 The land use values in the WOB basin model were obtained from the 2016 National Land  
234 Cover Database (NLCD), which contains 16 unique land classifications based on the modified  
235 Anderson Level II scheme (Yang et al., 2018). The NLCD land uses were re-classified to  
236 correspond with the five land use types used in the NSQD (see **Table S.2**). The removal efficiency

237 for each of the NBS types modeled in this study were obtained from the 2020 International  
238 Stormwater BMP Database (Clary et al., 2020), which corresponds well with average removal  
239 efficiencies in the NBS literature for watershed-scale stormwater modeling (e.g., Eckart et al.  
240 (2017); Liu et al. (2015)).

### 241 2.2.3 NBS Water Balance Modeling

242 EPA's SWMM engine calculates the water balance for NBS-driven systems using a nonlinear  
243 reservoir model (Chen and Shubinski, 1971) according to a unique set of infiltration, storage, and  
244 evaporation properties that describe, on a per-unit-area basis, how NBS structures impact  
245 hydrological behavior. A subset of zones and water fluxes as a function of NBS behavior is  
246 depicted in **Fig. 2**.



247  
248 **Fig. 2.** Conceptual model of NBS water balance processes.

249 The water fluxes are defined by Rossman and Huber (2016):

$$250 \quad \frac{\partial d_1}{\partial t} = q_0 - e_1 - f_1 - q_1, \quad (2)$$

$$251 \quad d_2 \frac{\partial \theta}{\partial t} = f_1 - e_2 - f_p, \quad (3)$$

$$252 \quad \frac{\partial d_3}{\partial t} = f_p - f_3 - q_3, \quad (4)$$

253 where  $d_1$  is the depth of ponded water on the surface zone with outflow  $q_1$  (cfs),  $d_2$  is the depth  
254 of the soil zone with moisture content  $\theta$ ,  $d_3$  is the depth of the storage zone with outflow  $q_3$  (cfs),  
255  $q_0$  describes the inflow to each NBS cell (cfs),  $e_1$  and  $e_2$  represent the evapotranspiration from the  
256 surface zone and the soil zone, respectively,  $f_1$  describes infiltration between the surface and soil  
257 zone,  $f_p$  is percolation between the soil and storage zone, and  $f_3$  is infiltration from the storage  
258 zone to the underdrain layer.

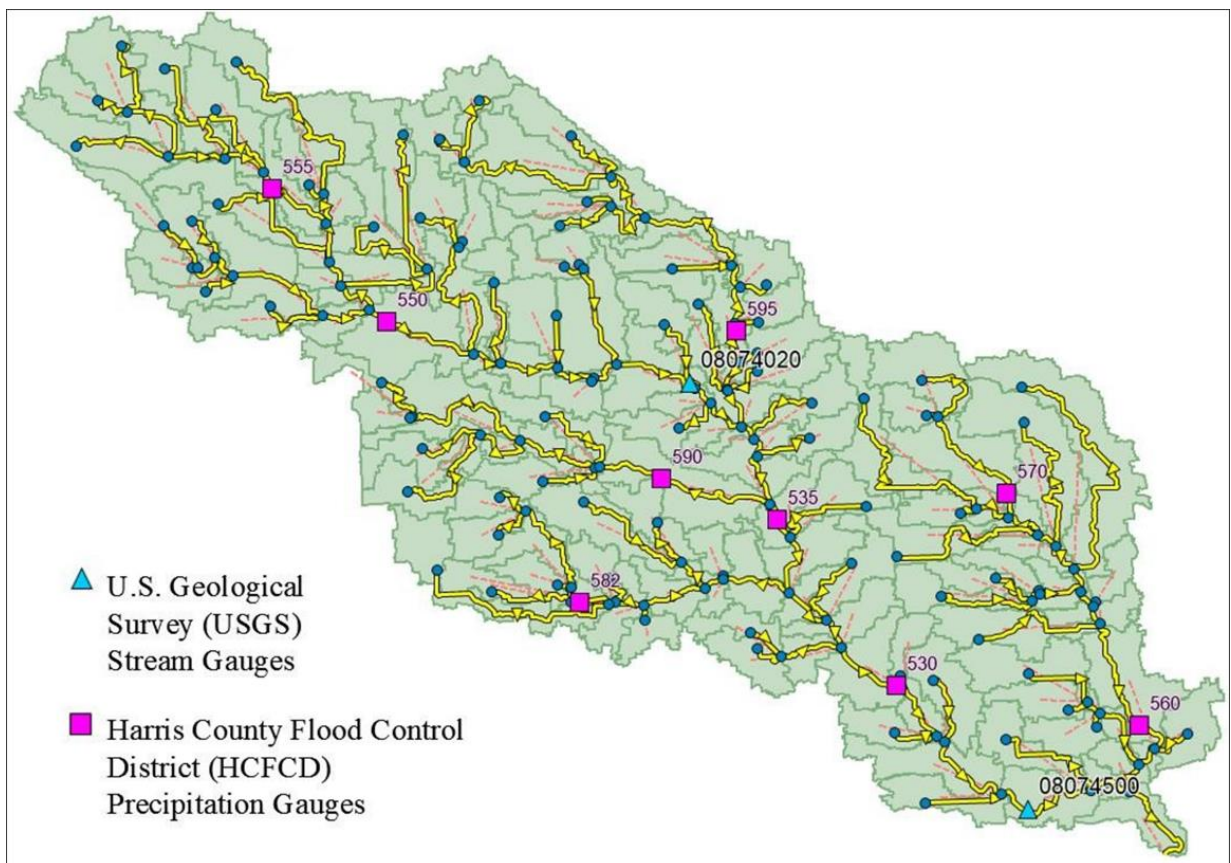
259 The flux terms ( $q$ ,  $e$ ,  $f$ ) are functions of the water content within each layer and subcatchment  
260 site conditions. The set of equations is solved at each runoff time step, according to the Green-  
261 Ampt method, to calculate how the inflow hydrograph to the NBS unit is converted to a runoff  
262 hydrograph, further described by Rossman (2014).

263 Within NBS systems, the surface zone represents the ground surface, which stores excess  
264 inflow and generates outflow either overland or to an adjacent drainage system. The soil zone is  
265 comprised of an engineered soil mixture that allows water to percolate into the underlying zone,  
266 which consists of rock and gravel for additional storage. The underdrain system conveys water out  
267 of the storage layer and into an engineered outlet. The three NBS features used in this case study  
268 (bioretention cells, porous pavement, and tree boxes) are summarized in **Table S.3** as a function  
269 of the representative water balance layers modeled in PCSWMM. In the WOB case study, tree  
270 boxes were modeled as bioretention cells with no outflow drain.

271 Various input parameters are also required within a SWMM model to describe the engineered  
272 design of local NBS features (e.g., conductivity rate, vegetation volume, clogging properties,  
273 surface roughness, etc.), which were obtained from the City of Houston design guidelines for low  
274 impact development (COH, 2019b), as summarized in **Table S.4**.

275 2.2.4 Calibration & Validation

276 The hydrological basin parameters were calibrated to observed streamflow measurements from  
277 United States Geological Survey (USGS) stream gauges #08074020 and #08074500 (USGS,  
278 2021a, 2021b). One year of daily precipitation values were obtained from the Harris County Flood  
279 Warning System (HCFWS) precipitation gauges #530, #535, #550, #555, #560, #570, #582, #590,  
280 and #595 (HCFCD, 2021), encompassing the totality of the White Oak Bayou watershed as shown  
281 in **Fig. 3**.



282

283 **Fig. 3.** PCSWMM basin model, stream gauges, and precipitation gauges for WOB.

284 The first six-months of precipitation data (October 2, 2020 – March 2, 2021) were used to  
285 calibrate the model, while the latter six-months of data (March 3, 2021 – August 2, 2021) were  
286 used to validate the model. The PCSWMM sensitivity-based radio tuning calibration (SRTC) tool

287 was used to aid in identifying the most sensitive parameters within the model, according to user-  
288 identified uncertainty, and for calibrating the model to match observed streamflow (CHI, 2015).  
289 The annual set of hydrographs for the basin model was disaggregated for wet weather conditions  
290 with a criterion of at least 500 cfs flow for a minimum of 4 consecutive hours (**Fig. S.1**), resulting  
291 in ten unique storm events for calibration (**Table S.5**) and eight unique storm events for validation  
292 (**Table S.6**). The wet weather flow hydrographs were calibrated using the PCSWMM SRTC tool  
293 by selecting uncertainties for control parameters based on their data source and sensitivity gradient,  
294 per guidelines proposed by Choi and Ball (2002) and James (2003). The gradients for the  
295 parameters with the greatest model sensitivity are shown in **Fig. S.2**. The basin model was then  
296 simulated with the calibrated parameters and compared to observed streamflow and resulting error  
297 metrics to measure goodness-of-fit (**Fig. S.3**).

298 The error metric employed in this study was the integrated square error (ISE), which  
299 amalgamates differences between observed and calibrated values according to overall storm runoff  
300 volume, peak flow, mean flow, and the hydrograph time to peak (James, 2003). The ISE is  
301 advantageous over the traditional Nash-Sutcliffe efficiency (NSE) or coefficient of determination  
302 ( $R^2$ ) because these latter error metrics are both sensitive to outliers and tend to converge on one  
303 measure of hydrological efficacy (i.e., total runoff *or* peak flow *or* average runoff) (CHI, 2020).  
304 The ISE is recommended for large-scale watershed planning due to its capability to assess  
305 goodness-of-fit over a range of historical rain events and hydrograph parameters, rather than  
306 potentially biasing the model to one specific event or metric of performance (CHI, 2015).  
307 Moreover, the ISE is beneficial in urban watersheds that are modeled without sub-surface flow  
308 because sewer system hydraulics may be indirectly calibrated using the ISE, whereas the NSE is  
309 dominated solely by overland flow conditions (Sarma et al., 1973).

310 The ISE is expressed as:

$$311 \quad ISE = \frac{\sqrt{\sum (y_{obs}^i - y_{comp}^i)^2}}{\sum y_{obs}^i}, \quad (5)$$

312 where  $y_{obs}^i$  is the observed value, and  $y_{comp}^i$  is the computed value for the  $i$ -th observation.

313 Then, the rating of the resulting ISE error metric may be defined on a qualitative scale, as defined  
314 by Sarma et al. (1973), such that  $ISE \leq 3 =$  Excellent,  $3 < ISE \leq 6 =$  Very Good,  $6 < ISE \leq 10 =$   
315 Good,  $10 < ISE \leq 25 =$  Fair, and  $ISE > 25 =$  Poor.

316 The model calibration and validation hydrographs and ISE error metrics are demonstrated in  
317 supplementary materials (**Fig. S.1 – Fig. S.3** and **Table S.5 – Table S.6**), respectively.

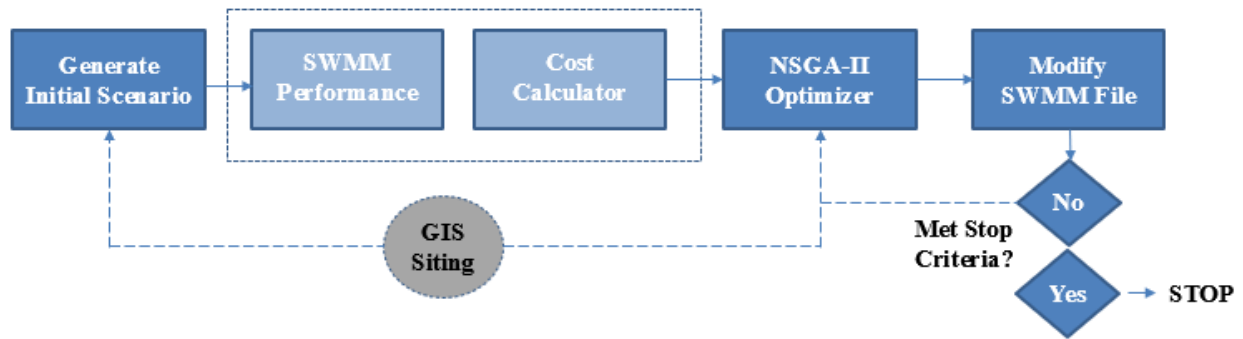
### 318 2.3 *Spatial Allocation Optimization*

319 A decision support tool, called GreenPlan-IT, was used to optimize the fully-calibrated  
320 watershed model according to levels of runoff reduction, pollutant load abatement, and cost  
321 effectiveness (Wu et al., 2019). The workflow for the optimization scheme is demonstrated in **Fig.**  
322 **4**, adapted from (SFEI, 2018). The optimization tool compares the performance of various NBS  
323 strategies to the baseline scenario, which represents watershed conditions prior to NBS  
324 implementation. Model performance is defined by three objectives: 1) minimized total relative  
325 cost of NBS implementation, 2) maximized reduction in hydrological runoff, and 3) maximized  
326 abatement of pollutant loads within the study area. GreenPlan-IT couples the nondominated sorting  
327 genetic algorithm (NSGA-II) with the EPA SWMM software according to the Pareto front solution  
328 (SFEI, 2018). The GreenPlan-IT package combines several unique tools that operate in succession  
329 to identify the optimal spatial allocation of NBS features, including:

- 330 1) GIS-based Site Locator Tool (SLT): Merges spatial characteristics of NBS types with  
331 regional geospatial information to identify all possible NBS locations within the study area.

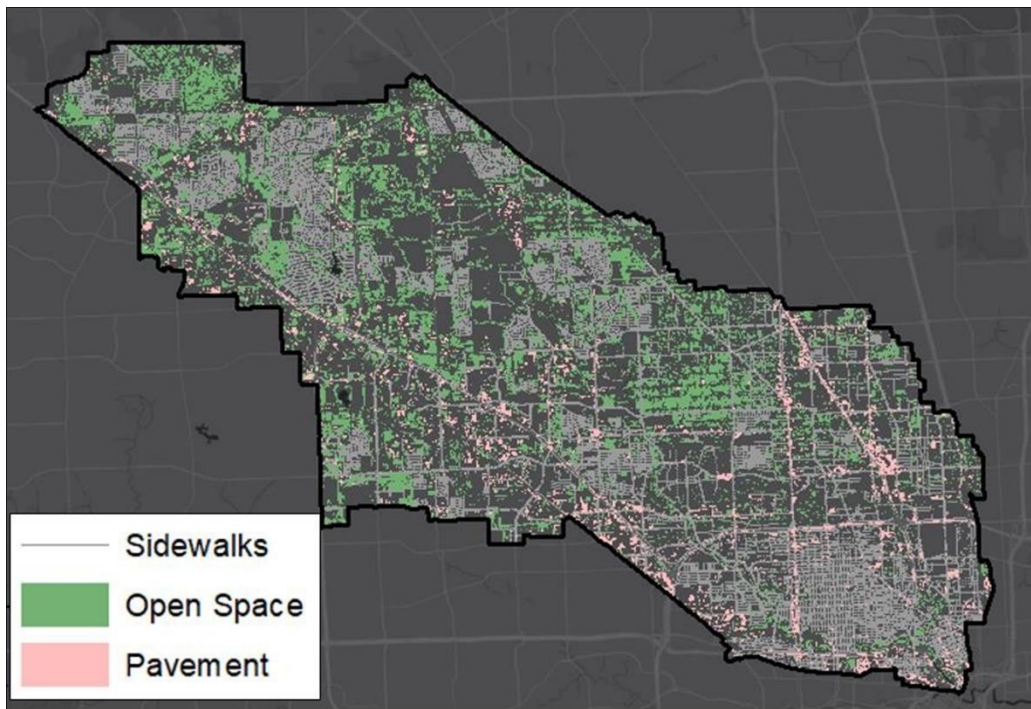


- 332 2) EPA SWMM Basin Model: Establishes baseline conditions for runoff and pollutant  
333 loading prior to NBS optimization.
- 334 3) GreenPlan-IT Optimization Tool (GPOT): An executable file that runs through the user's  
335 command prompt to identify optimal combinations of NBS types within each catchment  
336 area according to a cost-benefit analysis (where costs are defined by the user, and benefits  
337 are calculated using SWMM to assess the reduction in stormwater runoff and pollutant  
338 loads for many simulations).



339

340 **Fig. 4.** GreenPlan-IT optimization workflow.



341

342 **Fig. 5.** Geospatial siting of potential NBS locations in the WOB watershed.

343 The GIS-based SLT was used to identify all potential locations of NBS features within the  
344 WOB watershed, as shown in **Fig. 5**. Potential locations for bioretention cells, permeable

345 pavement, and tree boxes were defined according to open space land use parcels, areas of existing  
346 pavement, and adjacent land near existing sidewalks, respectively. Corresponding data layers were  
347 obtained from the City of Houston GIS Data Hub (COH, 2021). Baseline flow and TSS loads were  
348 quantified within the SWMM model for various design storm events, as described in **Section 2.2**.  
349 The SLT output serves as a spatial constraint for the GPOT, which executes several thousand  
350 SWMM models according to unique spatial allocations of NBS features within the permissible  
351 areas (i.e., the shaded areas shown in **Fig. 5**). The GPOT compares the performance of various  
352 NBS strategies to the baseline scenario, which represents watershed conditions prior to NBS  
353 implementation. Model performance is defined by three objectives: 1) minimized total relative  
354 cost of NBS implementation, 2) maximized reduction in hydrological runoff, and 3) maximized  
355 abatement of pollutant loads within the study area.

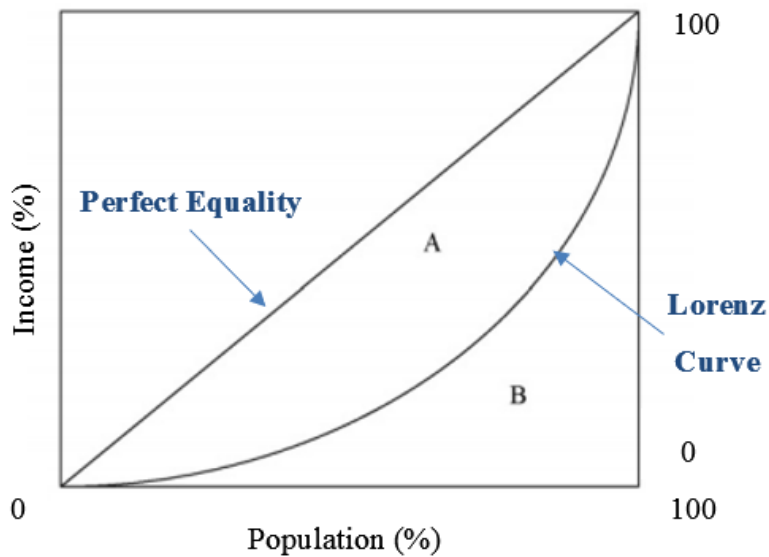
356 Relative cost estimates for the case study were obtained from the EPA National Stormwater  
357 Calculator (NSWC), which provides annual costs for NBS implementation and maintenance  
358 within unique geographical regions. At the time of study, the NSWC cost estimates for the  
359 Houston-area included: pervious pavement = \$8.68/SF, bioretention cells = \$6.07/SF, and tree  
360 planter boxes = \$9.46/SF (Bernagros et al., 2021). The GPOT uses two input files to compare NBS  
361 scenarios with the baseline SWMM model. The first input file contains the total acreage and  
362 percent impervious coverage for each subcatchment and the maximum number of possible NBS  
363 sites per subcatchment from the GIS-based SLT, as summarized in **Table S.7**. The second input  
364 file describes sizing parameters, where the NBS features were assigned a uniform unit area and  
365 width of 500 SF by 20 FT, 5000 SF by 50 FT, and 60 SF by 6 FT for bioretention cells, pervious  
366 pavements, and treeboxes, respectively.

367 The NSGA-II algorithm, originally presented by (Deb et al., 2002), searches for the optimal  
368 solution among numerous possible scenarios by first modeling a random set of NBS placements  
369 and comparing their outputs for non-dominance. Non-dominance occurs when a solution performs  
370 no worse than any other solution for all objectives (e.g., cost, runoff, and pollutant load efficiency)  
371 and also performs better than all other solutions within the cohort for at least one objective. This  
372 cohort (known as a generation), then sorts each of the sub-routines within the series (known as  
373 populations) for non-dominance. Another generation is run using the previous generation's non-  
374 dominant solutions and relative population samples. This iteration continues until the system either  
375 reaches a maximum number of generations or until no further changes are observed between two  
376 consecutive populations. The primary GreenPlan-IT tool, which was designed for use in the greater  
377 San Francisco Bay area, uses a threshold of 200 generations, each with a population size of 100,  
378 for a maximum of 20,000 watershed simulations (SFEI, 2018). The GreenPlan-IT tool was  
379 modified in concert with the tool developers for use in Houston, Texas, which resulted in an  
380 NSGA-II stop criteria of 100 generations, each with a population size of 250 model runs. As a  
381 result of this collaboration, it is our understanding that future versions of GreenPlan-IT will be  
382 released to allow application in other large watersheds, such as the WOB. The model outputs of  
383 the optimization tool are plotted as a function of cost (x-axis) versus runoff or load reduction (y-  
384 axis), resulting in a Pareto curve (see **Section 3.1**Error! Reference source not found.). Each point  
385 along the convex of the Pareto curve (known as the Pareto front) represents a unique, quasi-optimal  
386 solution for NBS spatial allocation according to the cost and reduction targets located on the Pareto  
387 curve axes (Wu et al., 2019).

#### 388 2.4 *Multi-objective Gini Index*

389 The Gini coefficient, which was originally identified by Gini (1912), is a statistical  
390 representation of inequality across a population. The Gini coefficient is based on the Lorenz curve,  
391 depicted in **Fig. 2**, which describes the cumulative proportion of values along the x-axis compared  
392 with the cumulative proportion of values along the y-axis. Within the social sciences, the Gini-  
393 based approach is commonly used to assess the degree of matching between population (x-axis)  
394 and income/wealth (y-axis) for economic purposes to quickly compare and rank disparate  
395 geographic entities (Giorgi and Gigliarano, 2017).

396 In a perfectly-equal scenario, the distribution of income matches the distribution of the  
397 population, shown as the diagonal line in **Fig. 2**. In a more realistic scenario, the normalized  
398 percentage of population to percentage of household income typically follows an exponential  
399 distribution, known as the Lorenz curve, which delineates state spaces **A** (e.g., the inequality gap)  
400 and **B** (e.g., the actual income distribution) in **Fig. 6**.



401  
402 **Fig. 2.** Conceptual graph of Gini-based equality and Lorenz curve.

403 The Gini coefficient ( $G$ ) is expressed graphically by

404 
$$G = \frac{A}{(A + B)}, \quad (6)$$

405 where  $A$  represents the total area between the line of equality and the Lorenz curve distribution,  
406 and  $B$  represents the area between the Lorenz curve and the base axes.

407 A numerical form of the Gini coefficient ( $G_i$ ) is given by

408 
$$G_i = 1 - \sum_{i=1}^n (Y_i - Y_{i-1})(X_i + X_{i-1}), \quad (7)$$

409 where  $X_i$  is the cumulative percentage of the variable on the x-axis, and  $Y_i$  is the cumulative  
410 percentage of the variable on the y-axis, for data point  $i$ , from  $i=1$  to  $i= n$  total data points.

411 Gini coefficient value ranges from 0 to 1, where 0 indicates absolute equality, and 1 represents  
412 absolute inequality. Due to the popularity of the Gini coefficient to quickly identify statistical  
413 differences in equality, studies have begun applying this economic concept to issues of energy  
414 allocation (Jacobson et al., 2005; Saboohi, 2001), environmental inequity (Boyce et al., 2016;  
415 Heerink et al., 2001; White, 2007), water resources allocation (Cho and Lee, 2014; Du et al., 2021;  
416 Hu et al., 2016; Yan et al., 2018), flood drainage rights (Zhang et al., 2020), and other topics  
417 regarding distribution of limited resources (Josa and Aguado, 2020).

418 Many of the recent applications of the Gini concept to issues of environmental concern utilize  
419 the area-based Gini coefficient. The area-based Gini (“AR-Gini”) compares a social metric,  
420 calculated on an area basis, to a distributed social good, calculated on a resource basis (Druckman  
421 and Jackson, 2008). The AR-Gini may be used to compare spatial patterns of space-based  
422 resources and population-based social metrics to reveal internal relationships, improve planning  
423 frameworks, and identify useful cross-disciplinary spatial indicators. An example of using the AR-  
424 Gini coefficient beyond the traditional scope of economic wealth disparity is given by Sun et al.  
425 (2010) where wastewater discharge permitting is optimized using the Gini index and a multi-

426 criteria assessment of land, population, income, and environmental capacity. In this study, the  
427 conflict between wastewater efficiency and social equality is bridged by balancing tradeoffs  
428 between various policy-making goals amidst limited resources (Sun et al., 2010).

429 The method presented here uses a novel representation of the AR-Gini to advance  
430 sustainability planning by combining hydrological, environmental, and social efficiencies within  
431 NBS spatial allocation optimization. In this study, the cumulative area of NBS allocation as a  
432 proportion of each subcatchment area is plotted on the y-axis, normalized on a scale from 0-100.  
433 Unique evaluation indicators (i.e., stormwater runoff, stormwater quality, and social equity) are  
434 then plotted on the x-axis, such that each potential optimization model contains three different Gini  
435 coefficients. Hydrological efficiency is represented as the percent difference of stormwater runoff  
436 volume between baseline and optimized conditions, as a function of cost. Environmental efficiency  
437 is described as the percent difference of pollutant load abatement between baseline and optimized  
438 conditions, according to cost. Social equity is a function of the average neighborhood disadvantage  
439 over the weighted area of NBS allocation within each subcatchment. By minimizing the sum of  
440 these multi-objective Gini coefficients, this novel approach reveals the state space of optimal  
441 hydrological efficacy and distribution of NBSs in socially-vulnerable locations.

442 Minimizing the Gini coefficient as a function of hydrological efficacy and social justice  
443 provides the novel framework for allocating NBSs according to both their hydrological  
444 functionality and also the social characteristics of persons that would be influenced by varying  
445 spatial arrangements. A high Gini coefficient would reveal that the distribution of NBSs using only  
446 hydrological efficacy does not maximize the multi-functional goals of improving societal health  
447 through improved access to nature. Here, several of the SWMM-based optimization scenarios from  
448 the GreenPlan-IT tool are calculated using the multi-functional Gini calculations, described below,

449 to better understand the trade-offs between hydro-environmental/economic efficiency and spatial  
450 equality when planning watershed-scale NBS solutions. The first objective is to maximize the  
451 economic benefit efficiency of hydro-environmental spatial optimization. The second objective is  
452 to maximize social equity using a composite AR-Gini coefficient. In doing so, a hypothesis is  
453 generated from robust hydro-dynamic modeling, which is then tested against the spatial  
454 representation of social deprivation to elicit a numerical hypothesis of holistic NBS conditions that  
455 are optimally distributed to maximize urban greening in areas of highest social vulnerability.

456 The following equations are applied in deriving the multi-objective Gini coefficient:

$$457 \quad \omega_s = \sum_{j=1}^n z_{js} A_j, \quad (8)$$

458 where  $\omega_s$  is the allocation of NBS area per subcatchment  $s$ ,  $n$  is number of unique NBS feature  
459 types  $j =$  bioretention cells, porous pavements, or tree boxes,  $z$  is the number NBSs per  
460 subcatchment,  $A_j$  is the area of each NBS feature type ( $A_j$ : bioretention cells = 500 SF, porous  
461 pavements = 5,000 SF, tree boxes = 60 SF),

$$462 \quad \eta_s = \frac{\left(\frac{a_s - b_s}{a_s}\right) * 100}{\sum_{j=1}^n z_{js} A_j c_j}, \quad (9)$$

463 where  $\eta_s$  is the percent efficiency of hydro-environmental improvement between the baseline  
464 model,  $a$ , and the optimized model,  $b$  for each subcatchment  $s$  as a function of the cost for each  
465 NBS feature,  $c_j$  ( $c_j =$  \$6.07/SF, \$8.68/SF, \$9.46/SF for  $j$ =bioretention cells, porous pavements,  
466 and tree boxes, respective);  $a$  and  $b$  represent the total stormwater runoff volume ( $V_R$ , in million  
467 gallons) for hydrologic efficiency and the total pollutant load runoff (TSS, in lbs) for  
468 environmental efficiency, from SWMM modeling.

$$469 \quad \mu_s = \frac{ADI_s}{\sum_{s=1}^m \omega_s}, \quad (10)$$

470 where  $\mu_s$  is the percent of social inequality addressed by the optimized model according to the  
471 total NBS allocated area within each subcatchment,  $\omega_s$ , for all subcatchments  $m$ , and the social  
472 inequality within the subcatchment is measured by the average spatial Area Deprivation Index  
473 (ADI) score within each subcatchment  $ADI_s$ .

474 To eliminate differences in measurement units and magnitudes among evaluation choices, each  
475 indicator is then normalized on a scale of 0 to 100 per

$$476 \quad \tilde{x} = \frac{x - x_{min}}{x_{max} - x_{min}} * 100, \quad (11)$$

477 where  $\tilde{x}$  is the normalized value of each  $x =$  hydrologic efficiency ( $\eta_s$ ), environmental efficiency  
478 ( $\eta_s$ ), and social equity ( $\mu_s$ ).

479 Consequently, the sum of the normalization series for each Lorenz curve axis is 100. The Gini  
480 coefficient is then calculated by:

$$481 \quad Y_s = Y_{s-1} + \frac{\tilde{\omega}_s}{\sum_{s=1}^m A_s} * 100, \quad (12)$$

$$482 \quad X_s = X_{s-1} + \left( \frac{\tilde{\eta}_s}{\sum_{s=1}^m \tilde{\eta}_s} \mid \frac{\tilde{\mu}_s}{\sum_{s=1}^m \tilde{\mu}_s} \right) * 100, \quad (13)$$

$$483 \quad G_i = 1 - \sum_{s=0}^m (X_s - X_{(s-1)})(Y_s - Y_{(s-1)}), \quad (14)$$

484 where  $Y_s$  is the y-axis value on the Lorenz curve,  $X_s$  is the x-axis value on the Lorenz curve,  $A_s$  is  
485 the area of each subcatchment  $s$ , with total subcatchments  $m$ , and  $G_i$  is the Gini coefficient  
486 corresponding to the evaluation index  $i =$  runoff volume efficiency, pollutant load efficiency, or  
487 social equity distribution.  $X_s$  and  $Y_s$  are plotted on the Lorenz curve by sorting  $Y_s$  in ascending  
488 order, where  $X_0$  and  $Y_0$  each equal 0.

489 Finally, the composite optimization objective is represented by



490 
$$\text{Optimization Objective: } \min \left( \frac{\sum_{i=1}^I G_i}{I} \right), \quad (5)$$

491 where  $G_i$  is the multi-functional Gini coefficient average for each indicator,  $i$ , for a total number  
492 of indicators  $I$ .

493 In summary, the following steps are applied to calculate the composite Gini index for  
494 amalgamating a series of NBS efficiency indicators according to both social deprivation and  
495 hydro-environmental risk:

- 496 1. Select a set of potential NBS allocation scenarios according to hydro-environmental  
497 SWMM-based optimization modeling.
- 498 2. Calculate Lorenz curve values for each efficiency indicator (hydrologic,  
499 environmental, and social) and NBS scenario.
- 500 3. Plot the Lorenz curves and calculate the individual Gini coefficients.
- 501 4. Aggregate the objective functions and compare Lorenz curves according to the multi-  
502 criteria Gini coefficient.
- 503 5. Identify the greatest distribution of social equality and hydro-environmental efficiency  
504 by minimizing the optimization objective function.

### 505 **3 Results and Discussion**

#### 506 *3.1 Hydro-environmental Pareto Front Curve*

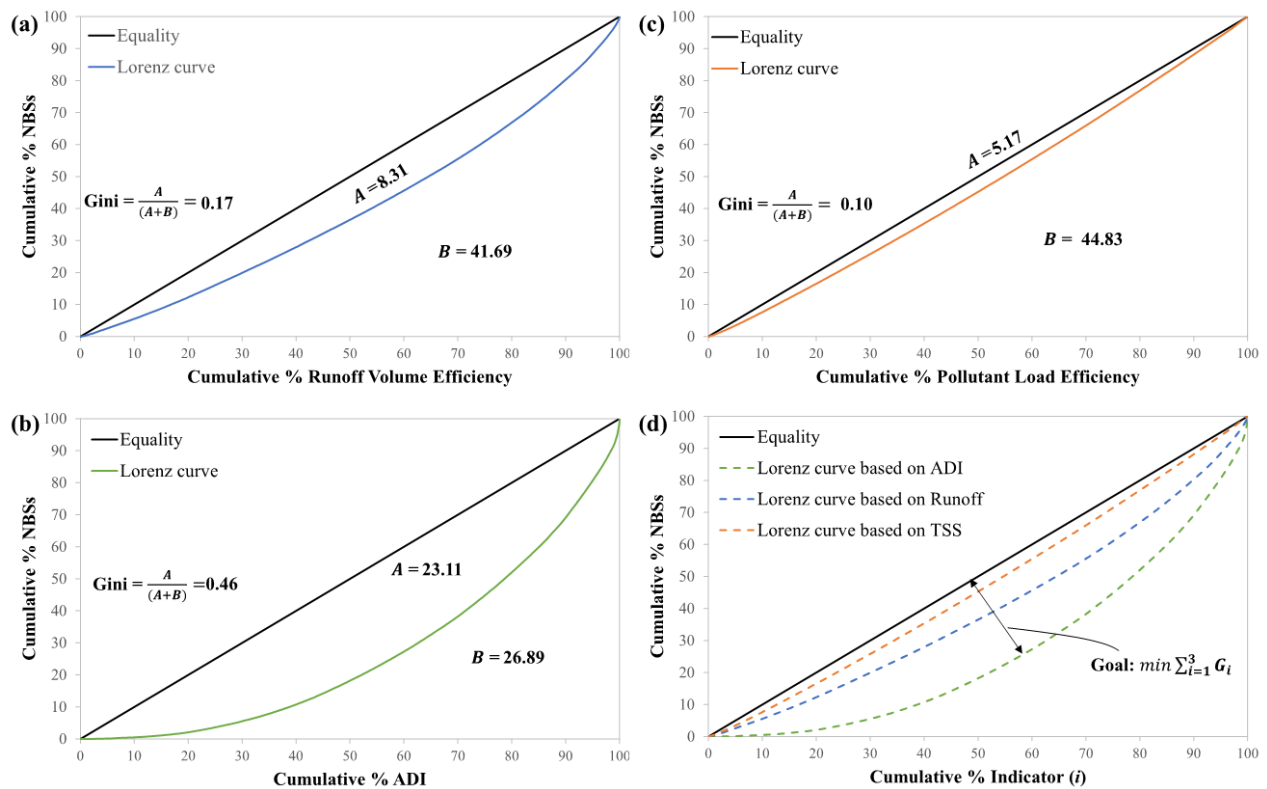
507 The GreenPlan-IT optimization tool for the WOB watershed converged after 100 generations  
508 (i.e., series), each with approximately 250 population values per generation. The 2-, 5-, and 100-  
509 year rainfall events were chosen as representative design storms for demonstrating the hydro-  
510 environmental optimization results, as demonstrated in **Fig.7**. An example of planning for NBS  
511 expenditure of \$1,000M is shown in the dashed lines where the optimal Pareto front results in a  
512 flow reduction of 3.22%, 3.62%, and 4.37% and a TSS pollutant load reduction 11.69%, 11.65%,  
513 and 9.55% of for the 2-, 5-, and 100-year design storms, respectively. The cost-effectiveness curves  
514 (i.e., the Pareto fronts) suggest there exists a largely linear relationship between the level of NBS

515 implementation and TSS pollutant load reduction between the 2-year and 5-year design storms.  
516 Decision-makers can then use these results to determine optimal NBS planning according to target  
517 expenditures. The cost-effectiveness curve in **Fig.** informs which Generation and Population  
518 model provides the most efficient hydro-environmental outcomes from the ~25,000 scenarios that  
519 were simulated in SWMM. By assessing the far-right portion of the Pareto front, decision-makers  
520 may identify at which point further investment in NBS technologies yield no additional  
521 improvement in hydro-environmental goals. As such, hydrologic versus environmental efficacy  
522 goals may be compared and contrasted between scenarios as a function of cost distribution and  
523 intensity of design storm metrics (SFEI, 2020). For example, if decision-makers had a goal of  
524 reducing the 100-YR storm flow by 5% (equating to a total cost of \$1,187M on the hydrologic  
525 cost-effectiveness curve), stakeholders could quickly visualize the flow reduction efficiency for  
526 additional design storms and the tradeoffs associated with pollutant load abatement at this cost  
527 point. To demonstrate how such optimization outputs may be combined with the multi-objective  
528 Gini coefficient described in **Sect. 2.4**, the 5-YR storm event with \$1,000M NBS expenditure was  
529 chosen for further analysis. In this scenario, Generation 97, Population 117 produced the most  
530 optimal NBS allocation scenario according to hydro-environmental efficiency. In comparing the  
531 spatial distribution of NBSs from this model with the areas of highest social deprivation in the  
532 WOB watershed, we may note how sole reliance upon hydrological characteristics for NBS  
533 planning could result in a missed opportunity to address potential social benefits from enhanced  
534 urban greening. As such, the multi-objective Gini is explored to refine the NBS optimization  
535 results.



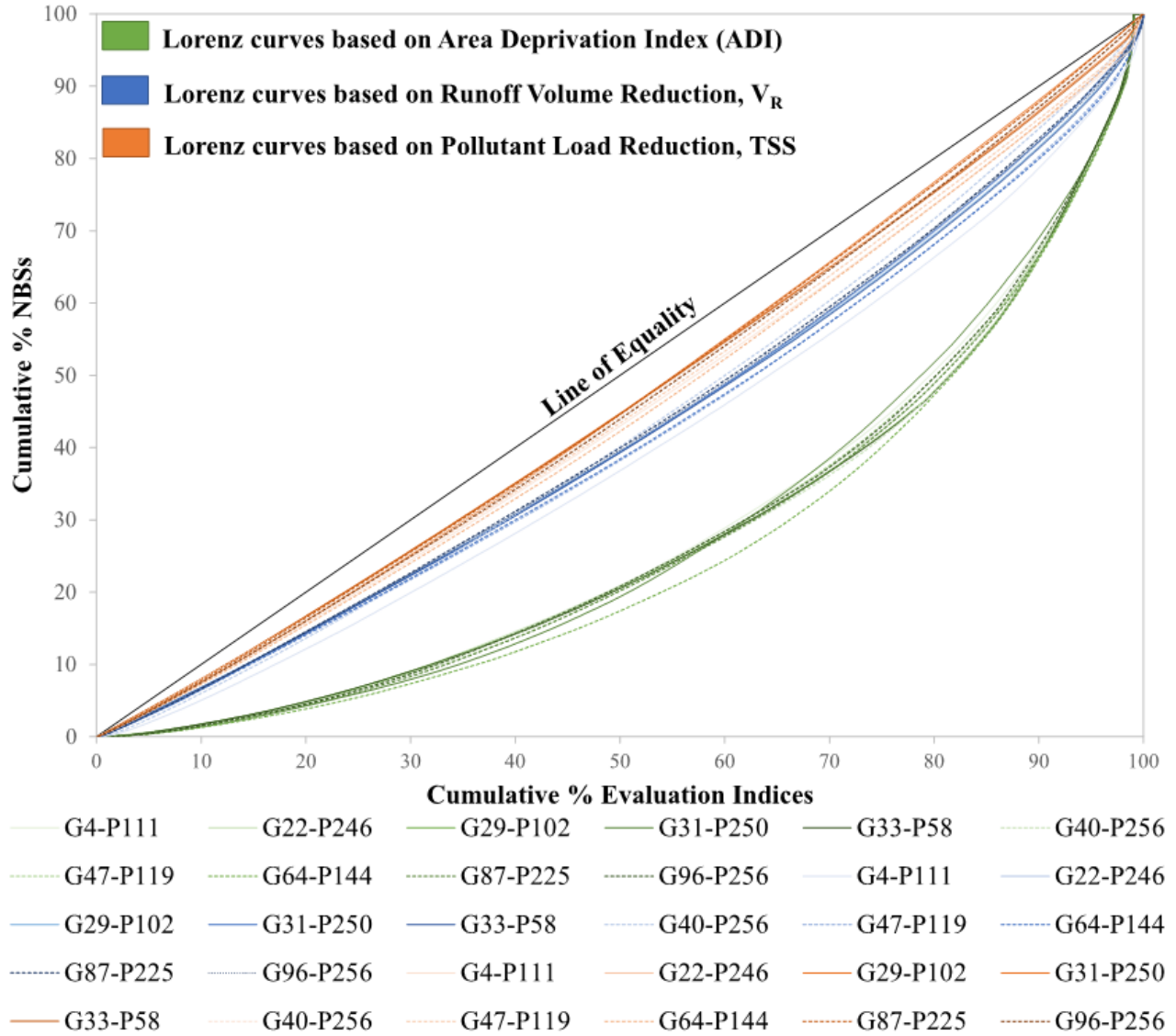
542 3.2 Gini-based Optimization

543 A Gini coefficient less than or equal to 0.4 is commonly used as a threshold denoting fair  
 544 distribution between the indicators on the x- and y-axes of the Lorenz curve (Groves-Kirkby et al.,  
 545 2009; Sadras and Bongiovanni, 2004). By plotting the Lorenz curves for the SWMM-based  
 546 optimization model (Generation 97, Population 117) in **Fig. 8**, the Gini coefficients according to  
 547 hydrologic efficiency, pollutant load efficiency, and social equity were calculate as 0.17, 0.10, and  
 548 0.46, respectively. Such results suggest a greater equity in NBS allocation on the basis of hydro-  
 549 dynamics compared with social characteristics. The large area between the Lorenz curve arc and  
 550 the line of equality in **Fig. 8c** reveals poor allocation fairness corresponding to spatial distribution  
 551 of neighborhood deprivation (i.e., the ADI index).



552  
 553 **Fig. 8.** Gini coefficients for Generation 97, Population 117 based on (a) runoff volume efficiency,  
 554 (b) pollutant load efficiency, (c) Area Deprivation Index, and (d) cumulative indicators.  
 555

556 A sample set of outputs from the GreenPlan-IT tool was selected from the 5-YR storm event,  
557 each resulting in a total NBS implementation cost of ~\$1,000M, to assess how the optimal  
558 allocation scheme may shift when the multi-objective Gini coefficient is applied. As shown in **Fig.**  
559 **9** and summarized in **Table 1**, a series of 10 possible NBS planning scenarios were evaluated on  
560 the basis of the composite Gini coefficient for hydrologic, environmental, and social indicators.  
561 By comparing the width of the Lorenz curves and minimizing the total Gini coefficient between  
562 these scenarios, **Fig. 9** reveals that the greatest distribution of equality occurs in planning scenario  
563 Generation 22, Population 246. The ideal Gini-based scheme provides a more equal distribution  
564 of overall benefits in comparison to the optimal scenario based solely on SWMM modeling  
565 ( $G_i=0.67$  in Generation 22, Population 246 and  $G_i=0.73$  in Generation 97, Population 117), despite  
566 a similar investment in financial resources. The construction of a multi-objective Lorenz curve is  
567 demonstrated here as a simple plot of cumulative NBS spatial allocation against cumulative  
568 evaluation indicators, allowing for easily interpretable comparisons across planning scenarios. The  
569 area between the Lorenz curve and the diagonal is proposed as a holistic index of socio-  
570 environmental-hydrological benefits in NBS planning. A larger area below the Lorenz curve  
571 suggests that the risk of stormwater-based metrics and social-based metrics are more variable  
572 within the planning paradigm, while a smaller area under the curve indicates a more uniform  
573 distribution of spatial planning for achieving multiple objectives. The Gini index is a  
574 straightforward calculation that could be used in NBS planning to merge holistic benefits using  
575 simple algebra. Since the coefficient of derivation under the Lorenz curve is calculated as a  
576 standard deviation according to the coefficient of variation, variation is relative, and thus invariant  
577 to changes in spatial scale. In other words, the Gini index provides a transparent measurement tool  
578 of the summary of impact fractions for optimal planning (Lee, 1997).



579

580 **Fig. 9.** Series of Lorenz curves for select 5-YR, ~\$1,000M optimization models.

581

582 **Table 1.** Multi-objective Gini coefficients for select 5-YR storm optimization series.

<b>Gen</b>	<b>G4</b>	<b>G22</b>	<b>G29</b>	<b>G31</b>	<b>G33</b>	<b>G40</b>	<b>G47</b>	<b>G64</b>	<b>G87</b>	<b>G96</b>
<b>Pop</b>	<b>P111</b>	<b>P246</b>	<b>P102</b>	<b>P250</b>	<b>P58</b>	<b>P256</b>	<b>P119</b>	<b>P144</b>	<b>P225</b>	<b>P256</b>
$G_{ADI}$	0.436	0.443	0.448	0.442	0.449	0.455	0.444	0.482	0.452	0.442
$G_{VR}$	0.210	0.157	0.161	0.158	0.163	0.146	0.179	0.178	0.150	0.155
$G_{TSS}$	0.108	0.072	0.078	0.074	0.080	0.081	0.097	0.112	0.073	0.086
$\sum G_i$	0.251	0.224	0.229	0.225	0.231	0.333	0.240	0.256	0.225	0.228

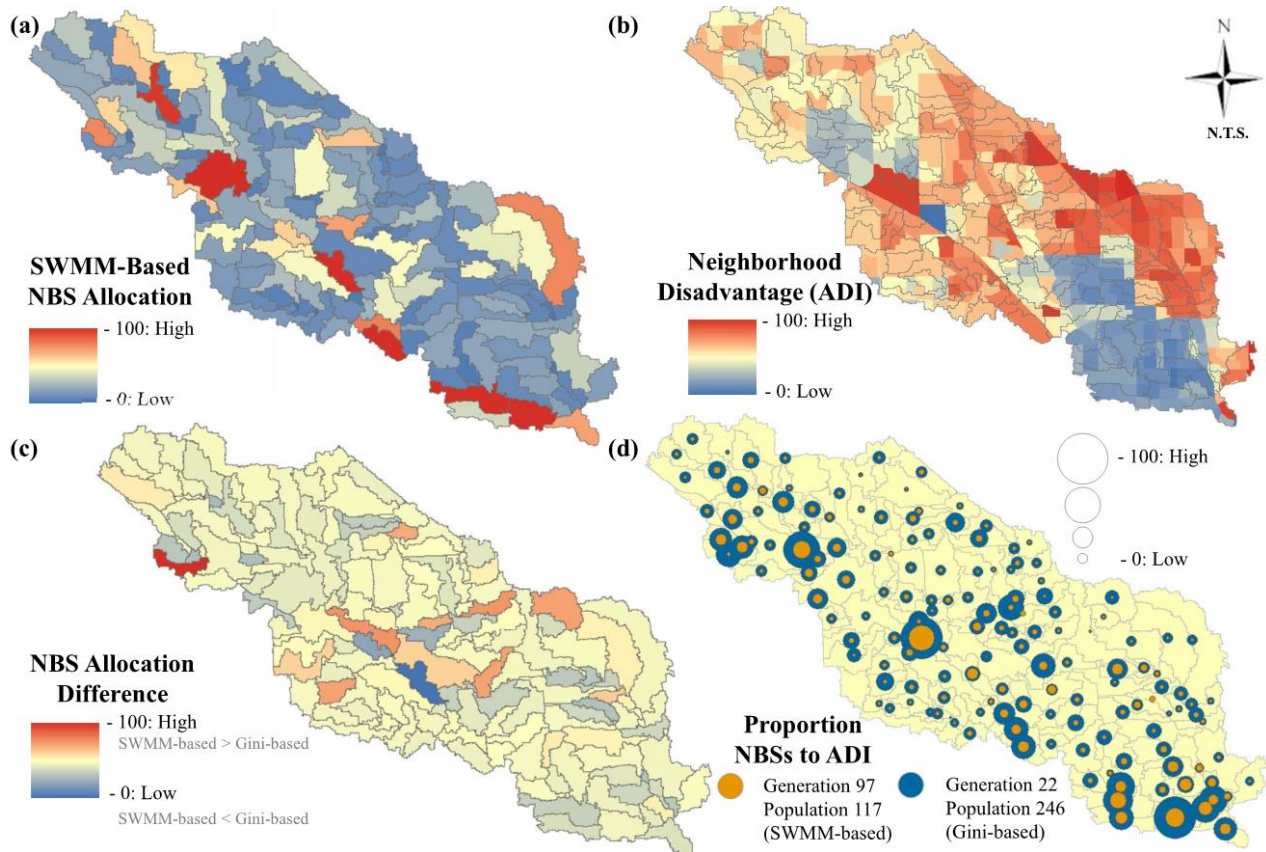
583

584 The optimal allocation of NBSs throughout the planning area may now be adjusted according

585 to the results of the composite Gini coefficient. In **Fig. 3**, the spatial distribution of NBS allocation

586 according to SWMM-based optimization (i.e., Generation 97, Population 117, from the Pareto  
587 front curve) is compared to the spatial distribution of NBSs from the Gini-based optimization (i.e.,  
588 Generation 22, Population 246, from the minimized composite  $G_i$ ). By plotting the subcatchments  
589 in each scenario as a weighted proportion of NBSs to ADI deprivation, **Fig. 3d** demonstrates a  
590 higher influence of NBS area on the allocation of social equity in the Gini-based scheme, thereby  
591 promoting improved societal conditions while maintaining robust hydro-environmental efficiency.  
592 As summarized in **Table** , both allocation scenarios produce similar runoff volume and pollutant  
593 load reduction benefits for roughly the same implementation cost. However, the unique spatial  
594 allocation of the NBS features within the Gini-based scenario addresses an additional 18.48% of  
595 land areas with high neighborhood disadvantage, as measured by the ADI index.

596 The pattern of total allocation of benefits between the SWMM-based and the Gini-based  
597 framework is further demonstrated in **Fig. 41**, where the pie charts represent the weighted  
598 efficiency achieved in each subcatchment according to hydrologic, environmental, and social  
599 aspects. The green portions of the pie charts in **Fig. 41** reveals a greater influence of NBS allocation  
600 to ADI improvement in Generation 22, Population 246. The primary reason for this disparity is  
601 that areas highly prone to flooding or environmental quality issues are not always spatially  
602 proportional to areas of high social deprivation. As such, reliance upon a “worst-first” approach to  
603 NBS planning through the lens of hydro-dynamics may result in non-optimal allocation for  
604 addressing the many societal benefits provided by NBS solutions.



605

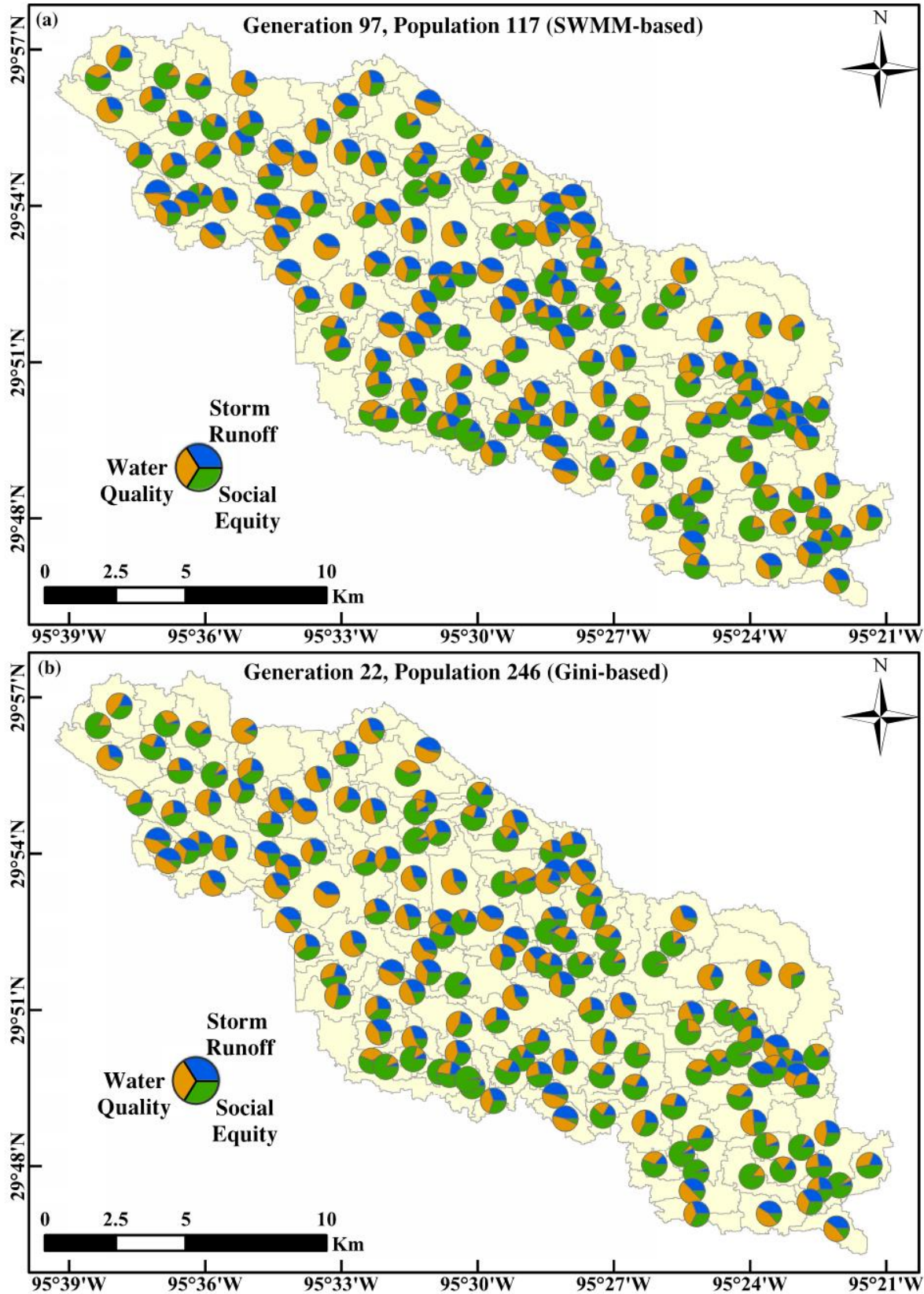
606 **Fig. 30.** Comparison of spatial distribution in the WOB watershed for (a) NBS allocation  
 607 according to optimal hydro-environmental efficiency (Generation 97, Population 117), (b) areas  
 608 of neighborhood disadvantage, represented by the Area Deprivation Index (ADI), (c) difference  
 609 between NBS allocation for SWMM-based optimization (Generation 97, Population 117) versus  
 610 Gini-based optimization (Generation 22, Population 246), and (d) weighted proportion of NBS  
 611 allocation within each subcatchment compared to ADI deprivation metrics.  
 612

613 **Table 2.** Comparison of SWMM-based optimized model versus Gini-based optimized model.

	<b>G97 P117</b>	<b>G22 P246</b>
Cost (\$M)	\$1006	\$1000
Runoff Volume Reduction	3.45%	3.38%
Pollutant Load Reduction	11.15%	11.28%
No. Bioretention Cells	168,459	189,385
No. Porous Pavements	8,705	7,772
No. Tree Boxes	239,001	154,824
% ADI Addressed by NBSs	16.84%	35.32%

614





615  
616  
617

**Fig. 41.** Proportional representation of evaluation indicator efficiency for (a) SWMM-based optimization model, and (b) Gini-based optimization model.

618 **4 Conclusion**

619 NBS design is a function of rapid urban development, quality of life goals, and a scarcity of  
620 resources for addressing hydro-meteorological challenges. As such, proper co-development of  
621 NBS plans can and should account for the multi-functional components involved in all of these  
622 processes, and we must do so in a coherent fashion for optimal impact in the coming era of water  
623 science. While coupled social and physical models have proliferated within the general realm of  
624 water security (e.g., droughts, water use, hydro-meteorological hazards, migration, agriculture,  
625 etc.), the foundation of such a framework has been hitherto lacking within the NBS scientific  
626 literature. In considering the rising popularity of urban green infrastructure, we are presented with  
627 an opportunity to re-cast how decision-making operates in order to maximize the numerous co-  
628 benefits associated with NBSs. As resilience and sustainability goals have become increasingly  
629 linked, many governmental agencies are seeking the prioritization of NBS capital improvement  
630 projects using an equity-based or benefits-based prioritization metric to help guide holistic  
631 investments rather than focusing in a one dimensional benefit (Marchese et al., 2018).

632 In this light, strategic NBS planning requires real-world empirical datasets (e.g., social  
633 vulnerability, watershed properties) and actionable frameworks (e.g., equity-based planning) to  
634 aid in optimal planning amongst disparate social and physical domains (Frantzeskaki,  
635 McPhearson, Collier, et al., 2019). When we are better able to select the optimal location of NBSs  
636 at the watershed-scale, the specific typologies and precise placement may be analyzed using the  
637 numerous platforms that currently operate through small-scale physical modeling (e.g., EPA's  
638 SWMM). To date, there has been very little research on NBS optimization at the watershed-scale  
639 and even less progress in combining numerical modeling with comprehensive social benefits and  
640 human impacts. As we continue to have increased access to heterogenous datasets, novel

641 frameworks that leverage the strengths of geospatial properties will enhance our understanding of  
642 diverse co-benefits to answer challenging questions associated with multi-functional planning.

643 As such, we demonstrated here how real-world social and hydro-environmental complexities  
644 may be amalgamated using a novel application of the area Gini coefficient for actionable science.  
645 The White Oak Bayou case study investigated how social equity and watershed dynamics  
646 propagate throughout the NBS system, which is fundamental to planning for an equitable  
647 environment. This study harmonized multi-indicator planning by facilitating an explicit integration  
648 of social determinants within the framework of natural-planning using data-driven science. This  
649 research transitioned beyond the standard focus of watershed physiological characteristics to  
650 investigate the complex associations relating social patterns and watershed efficacy.

651 The practical implications of this study will enhance the user-friendliness of NBS spatial  
652 planning in a flexible manner while merging well-established hydrological methodologies with  
653 social co-benefits (Kuller et al., 2017). When we are better able to connect the dots between social  
654 constructs, environmental processes, and the hydrological cycle, which are all complex processes  
655 that operate cohesively amongst one another, we can establish optimal patterns within the  
656 seemingly chaotic network of NBS sub-processes. By constructing models with inter-disciplinary  
657 elements, the foundation for novel research regarding how NBSs function in diverse geographical  
658 locations is strengthened. In a world with increasing socio-environmental stressors and finite  
659 resources, this research will improve public policy interventions by providing the knowledge  
660 necessary for identifying, quantifying, and linking complex interactions of NBS functions for  
661 sound decision-making.

662 **Declaration of Competing Interest**

663 The author declares that they have no known competing financial interests or personal  
664 relationships that could have appeared to influence the work reported in this paper.

665 **Acknowledgements**

666 The author thanks the efforts provided by Dr. Tan Zi of the San Francisco Estuary Institute  
667 (SFEI) for troubleshooting the GreenPlan-IT optimization tool to allow application to a large  
668 regional watershed in Houston, TX, USA.

669 **References**

- 670 Addala, A., Auzanneau, M., Miller, K., Maier, W., Foster, N., Kapellen, T., Walker, A., Rosenbauer, J., Maahs, D.M., Holl,  
671 R.W., 2021. A decade of disparities in diabetes technology use and HBA1c in pediatric type 1 diabetes: A transatlantic  
672 comparison. *Diabetes Care* 44. <https://doi.org/10.2337/dc20-0257>
- 673 Adib, M., Wu, H., 2020. Fostering community-engaged green stormwater infrastructure through the use of participatory  
674 geographic information systems (PGIS). *J. Digit. Landsc. Archit.* 2020. <https://doi.org/10.14627/537690056>
- 675 Alves, A., Gersonius, B., Kapelan, Z., Vojinovic, Z., Sanchez, A., 2019. Assessing the Co-Benefits of green-blue-grey  
676 infrastructure for sustainable urban flood risk management. *J. Environ. Manage.* 239.  
677 <https://doi.org/10.1016/j.jenvman.2019.03.036>
- 678 Astell-Burt, T., Feng, X., 2021. Urban green space, tree canopy and prevention of cardiometabolic diseases: A multilevel  
679 longitudinal study of 46 786 Australians. *Int. J. Epidemiol.* 49. <https://doi.org/10.1093/IJE/DYZ239>
- 680 Barco, J., Wong, K.M., Stenstrom, M.K., 2009. Closure to “Automatic Calibration of the US EPA SWMM Model for a Large  
681 Urban Catchment” by Janet Barco, Kenneth M. Wong, and Michael K. Stenstrom. *J. Hydraul. Eng.* 135.  
682 [https://doi.org/10.1061/\(asce\)hy.1943-7900.0000121](https://doi.org/10.1061/(asce)hy.1943-7900.0000121)
- 683 Barrett, D., 2019. NOAA Atlas 14 PCPM IDF Curves Update.
- 684 Bernagros, J.T., Pankani, D., Struck, S.D., Deerhake, M.E., 2021. Estimating Regionalized Planning Costs of Green  
685 Infrastructure and Low-Impact Development Stormwater Management Practices: Updates to the US Environmental  
686 Protection Agency’s National Stormwater Calculator. *J. Sustain. Water Built Environ.* 7.  
687 <https://doi.org/10.1061/jswbay.0000934>
- 688 Blair, P., Buytaert, W., 2016. Socio-hydrological modelling: A review asking “why, what and how?” *Hydrol. Earth Syst. Sci.* 20.  
689 <https://doi.org/10.5194/hess-20-443-2016>
- 690 Bouziotas, D., Ertsen, M., 2017. Socio-hydrology from the bottom up: A template for agent-based modeling in irrigation systems.  
691 *Hydrol. Earth Syst. Sci. Discuss.* <https://doi.org/10.5194/hess-2017-107>
- 692 Boyce, J.K., Zwickl, K., Ash, M., 2016. Measuring environmental inequality. *Ecol. Econ.* 124.  
693 <https://doi.org/10.1016/j.ecolecon.2016.01.014>
- 694 Brown, S.C., Lombard, J., Wang, K., Byrne, M.M., Toro, M., Plater-Zyberk, E., Feaster, D.J., Kardys, J., Nardi, M.I., Perez-  
695 Gomez, G., Pantin, H.M., Szapocznik, J., 2016. Neighborhood greenness and chronic health conditions in medicare  
696 beneficiaries. *Am. J. Prev. Med.* 51. <https://doi.org/10.1016/j.amepre.2016.02.008>
- 697 Castro, C. V., Maidment, D.R., 2020. GIS preprocessing for rapid initialization of HEC-HMS hydrological basin models using  
698 web-based data services. *Environ. Model. Softw.* 130. <https://doi.org/10.1016/j.envsoft.2020.104732>
- 699 Chamberlain, A.M., Finney Rutten, L.J., Wilson, P.M., Fan, C., Boyd, C.M., Jacobson, D.J., Rocca, W.A., St Sauver, J.L., 2020.  
700 Neighborhood socioeconomic disadvantage is associated with multimorbidity in a geographically-defined community.  
701 *BMC Public Health* 20. <https://doi.org/10.1186/s12889-019-8123-0>

Non-peer reviewed EarthArXiv preprint.  
Under review by *Journal of Hydrology*

- 702 Chen, C.W., Shubinski, R.P., 1971. Computer Simulation of Urban Storm Water Runoff. *J. Hydraul. Div.* 97.  
703 <https://doi.org/10.1061/jyceaj.0002871>
- 704 CHI, 2020. PCSWMM Support Manual: Error Functions.
- 705 CHI, 2015. PCSWMM User's Manual Support: Sensitivity-based Radio Tuning Calibration (SRTC).
- 706 CHI, 2014. PCSWMM Support: Transect creator.
- 707 Cho, J.H., Lee, J.H., 2014. Multi-objective waste load allocation model for optimizing waste load abatement and inequality  
708 among waste dischargers. *Water. Air. Soil Pollut.* 225. <https://doi.org/10.1007/s11270-014-1892-2>
- 709 Choi, K.S., Ball, J.E., 2002. Parameter estimation for urban runoff modelling. *Urban Water* 4. <https://doi.org/10.1016/S1462->  
710 [0758\(01\)00072-3](https://doi.org/10.1016/S1462-0758(01)00072-3)
- 711 Clary, J., Leisenring, M., Strecker, E., 2020. International Stormwater BMP Database: 2020 Summary Statistics.
- 712 COH, 2021. City of Houston Data Hub.
- 713 COH, 2019a. Infrastructure Design Manual 2019, Section 9.2.01.B.1, Design Rainfall Events.
- 714 COH, 2019b. City of Houston Design Manual: Chapter 9, Stormwater Design Requirements, Section 9.15.
- 715 Deb, K., Pratap, A., Agarwal, S., Meyarivan, T., 2002. A fast and elitist multiobjective genetic algorithm: NSGA-II. *IEEE Trans.*  
716 *Evol. Comput.* 6. <https://doi.org/10.1109/4235.996017>
- 717 Despart, Z., 2019. Harris County approves "worst-first" priority model for flood bond projects.
- 718 Druckman, A., Jackson, T., 2008. Measuring resource inequalities: The concepts and methodology for an area-based Gini  
719 coefficient. *Ecol. Econ.* 65. <https://doi.org/10.1016/j.ecolecon.2007.12.013>
- 720 Du, E., Cai, X., Wu, F., Foster, T., Zheng, C., 2021. Exploring the impacts of the inequality of water permit allocation and  
721 farmers' behaviors on the performance of an agricultural water market. *J. Hydrol.* 599.  
722 <https://doi.org/10.1016/j.jhydrol.2021.126303>
- 723 Eckart, K., McPhee, Z., Bolisetti, T., 2017. Performance and implementation of low impact development – A review. *Sci. Total*  
724 *Environ.* <https://doi.org/10.1016/j.scitotenv.2017.06.254>
- 725 Fenner, R., 2017. Spatial evaluation of multiple benefits to encourage multi-functional design of sustainable drainage in Blue-  
726 Green cities. *Water (Switzerland)* 9. <https://doi.org/10.3390/w9120953>
- 727 Flanagan, B.E., Gregory, E.W., Hallisey, E.J., Heitgerd, J.L., Lewis, B., 2020. A Social Vulnerability Index for Disaster  
728 Management. *J. Homel. Secur. Emerg. Manag.* 8. <https://doi.org/10.2202/1547-7355.1792>
- 729 Frantzeskaki, N., McPhearson, T., Collier, M.J., Kendal, D., Bulkeley, H., Dumitru, A., Walsh, C., Noble, K., Van Wyk, E.,  
730 Ordóñez, C., Oke, C., Pintér, L., 2019. Nature-based solutions for urban climate change adaptation: Linking science,  
731 policy, and practice communities for evidence-based decision-making. *Bioscience* 69.  
732 <https://doi.org/10.1093/biosci/biz042>
- 733 Fuertes, E., Markevych, I., von Berg, A., Bauer, C.P., Berdel, D., Koletzko, S., Sugiri, D., Heinrich, J., 2014. Greenness and  
734 allergies: Evidence of differential associations in two areas in Germany. *J. Epidemiol. Community Health* 68.  
735 <https://doi.org/10.1136/jech-2014-203903>
- 736 Gascon, M., Triguero-Mas, M., Martínez, D., Dadvand, P., Rojas-Rueda, D., Plasència, A., Nieuwenhuijsen, M.J., 2016.  
737 Residential green spaces and mortality: A systematic review. *Environ. Int.* <https://doi.org/10.1016/j.envint.2015.10.013>
- 738 Gini, C.W., 1912. Variability and Mutability, contribution to the study of statistical distributions and relations. *Stud. Econ. della*  
739 *Stud. Econ. della R. Univ. Cagliari.*
- 740 Giorgi, G.M., Gliarano, C., 2017. THE GINI CONCENTRATION INDEX: A REVIEW OF THE INFERENCE  
741 LITERATURE. *J. Econ. Surv.* 31. <https://doi.org/10.1111/joes.12185>
- 742 Golden, H.E., Hoghooghi, N., 2018. Green infrastructure and its catchment-scale effects: an emerging science. *Wiley Interdiscip.*  
743 *Rev. Water* 5. <https://doi.org/10.1002/wat2.1254>
- 744 Groves-Kirkby, C.J., Denman, A.R., Phillips, P.S., 2009. Lorenz Curve and Gini Coefficient: Novel tools for analysing seasonal  
745 variation of environmental radon gas. *J. Environ. Manage.* 90. <https://doi.org/10.1016/j.jenvman.2009.01.003>
- 746 Hamouz, V., Møller-Pedersen, P., Muthanna, T.M., 2020. Modelling runoff reduction through implementation of green and grey  
747 roofs in urban catchments using PCSWMM. *Urban Water J.* 17. <https://doi.org/10.1080/1573062X.2020.1828500>
- 748 HCFCD, 2021. Harris County Flood Warning System.
- 749 HCFCD, 2019. Model and map management system (M3). Harris Cty. Flood Control Dist.
- 750 Heerink, N., Mulatu, A., Bulte, E., 2001. Income inequality and the environment: Aggregation bias in environmental Kuznets

- 751 curves. *Ecol. Econ.* 38. [https://doi.org/10.1016/S0921-8009\(01\)00171-9](https://doi.org/10.1016/S0921-8009(01)00171-9)
- 752 Hirshberg, E.L., Wilson, E.L., Stanfield, V., Kuttler, K.G., Majercik, S., Beesley, S.J., Orme, J., Hopkins, R.O., Brown, S.M.,  
753 2019. Impact of Critical Illness on Resource Utilization: A Comparison of Use in the Year Before and After ICU  
754 Admission. *Crit. Care Med.* 47. <https://doi.org/10.1097/CCM.0000000000003970>
- 755 Hu, Z., Chen, Y., Yao, L., Wei, C., Li, C., 2016. Optimal allocation of regional water resources: From a perspective of equity-  
756 efficiency tradeoff. *Resour. Conserv. Recycl.* 109. <https://doi.org/10.1016/j.resconrec.2016.02.001>
- 757 Ingraham, N.E., Purcell, L.N., Karam, B.S., Dudley, R.A., Usher, M.G., Warlick, C.A., Allen, M.L., Melton, G.B., Charles, A.,  
758 Tignanelli, C.J., 2021. Racial and Ethnic Disparities in Hospital Admissions from COVID-19: Determining the Impact of  
759 Neighborhood Deprivation and Primary Language. *J. Gen. Intern. Med.* <https://doi.org/10.1007/s11606-021-06790-w>
- 760 Jacobson, A., Milman, A.D., Kammen, D.M., 2005. Letting the (energy) Gini out of the bottle: Lorenz curves of cumulative  
761 electricity consumption and Gini coefficients as metrics of energy distribution and equity. *Energy Policy* 33.  
762 <https://doi.org/10.1016/j.enpol.2004.02.017>
- 763 James, W., 2003. Rules for responsible modeling.
- 764 Jato-Espino, D., Charlesworth, S.M., Bayon, J.R., Warwick, F., 2016. Rainfall-runoff simulations to assess the potential of suds  
765 for mitigating flooding in highly urbanized catchments. *Int. J. Environ. Res. Public Health* 13.  
766 <https://doi.org/10.3390/ijerph13010149>
- 767 Josa, I., Aguado, A., 2020. Measuring Unidimensional Inequality: Practical Framework for the Choice of an Appropriate  
768 Measure. *Soc. Indic. Res.* 149. <https://doi.org/10.1007/s11205-020-02268-0>
- 769 Kabisch, N., Frantzeskaki, N., Pauleit, S., Naumann, S., Davis, M., Artmann, M., Haase, D., Knapp, S., Korn, H., Stadler, J.,  
770 Zaubringer, K., Bonn, A., 2016. Nature-based solutions to climate change mitigation and adaptation in urban areas:  
771 Perspectives on indicators, knowledge gaps, barriers, and opportunities for action. *Ecol. Soc.* 21.  
772 <https://doi.org/10.5751/ES-08373-210239>
- 773 Kandakoglu, A., Frini, A., Ben Amor, S., 2019. Multicriteria decision making for sustainable development: A systematic review.  
774 *J. Multi-Criteria Decis. Anal.* 26. <https://doi.org/10.1002/mcda.1682>
- 775 Kind, A.J.H., Buckingham, W.R., 2018. Making Neighborhood-Disadvantage Metrics Accessible — The Neighborhood Atlas.  
776 *N. Engl. J. Med.* 378. <https://doi.org/10.1056/nejmp1802313>
- 777 Knighton, A.J., Savitz, L., Belnap, T., Stephenson, B., VanDerslice, J., 2016. Introduction of an Area Deprivation Index  
778 Measuring Patient Socio-economic Status in an Integrated Health System: Implications for Population Health. *eGEMS*  
779 (Generating Evid. Methods to Improv. patient outcomes) 4. <https://doi.org/10.13063/2327-9214.1238>
- 780 Koutsoyiannis, D., Kozonis, D., Manetas, A., 1998. A mathematical framework for studying rainfall intensity-duration-frequency  
781 relationships. *J. Hydrol.* 206. [https://doi.org/10.1016/S0022-1694\(98\)00097-3](https://doi.org/10.1016/S0022-1694(98)00097-3)
- 782 Kuil, L., Carr, G., Viglione, A., Prskawetz, A., Blöschl, G., 2016. Conceptualizing socio-hydrological drought processes: The  
783 case of the Maya collapse. *Water Resour. Res.* 52. <https://doi.org/10.1002/2015WR018298>
- 784 Kuller, M., Bach, P.M., Ramirez-Lovering, D., Deletic, A., 2017. Framing water sensitive urban design as part of the urban form:  
785 A critical review of tools for best planning practice. *Environ. Model. Softw.* <https://doi.org/10.1016/j.envsoft.2017.07.003>
- 786 Kurani, S.S., McCoy, R.G., Lampman, M.A., Doubeni, C.A., Finney Rutten, L.J., Inselman, J.W., Giblon, R.E., Bunkers, K.S.,  
787 Stroebel, R.J., Rushlow, D., Chawla, S.S., Shah, N.D., 2020. Association of Neighborhood Measures of Social  
788 Determinants of Health With Breast, Cervical, and Colorectal Cancer Screening Rates in the US Midwest. *JAMA Netw.*  
789 *open* 3. <https://doi.org/10.1001/jamanetworkopen.2020.0618>
- 790 Lee, W.C., 1997. Characterizing exposure-disease association in human populations using the Lorenz curve and Gini index. *Stat.*  
791 *Med.* 16. [https://doi.org/10.1002/\(SICI\)1097-0258\(19970415\)16:7<729::AID-SIM491>3.0.CO;2-A](https://doi.org/10.1002/(SICI)1097-0258(19970415)16:7<729::AID-SIM491>3.0.CO;2-A)
- 792 Li, H., Ding, L., Ren, M., Li, C., Wang, H., 2017. Sponge city construction in China: A survey of the challenges and  
793 opportunities. *Water (Switzerland)* 9. <https://doi.org/10.3390/w9090594>
- 794 Lim, T.C., Welty, C., 2017. Effects of spatial configuration of imperviousness and green infrastructure networks on hydrologic  
795 response in a residential sewershed. *Water Resour. Res.* 53. <https://doi.org/10.1002/2017WR020631>
- 796 Lin, J., 2004. Review of published export coefficient and event mean concentration (EMC) data: ERDC TN-WRAP-04-3.
- 797 Link, B.G., Phelan, J., 1995. Social conditions as fundamental causes of disease. *J. Health Soc. Behav.*  
798 <https://doi.org/10.2307/2626958>
- 799 Liu, L., Jensen, M.B., 2018. Green infrastructure for sustainable urban water management: Practices of five forerunner cities.  
800 *Cities* 74. <https://doi.org/10.1016/j.cities.2017.11.013>
- 801 Liu, Y., Ahiablame, L.M., Bralts, V.F., Engel, B.A., 2015. Enhancing a rainfall-runoff model to assess the impacts of BMPs and

- 802 LID practices on storm runoff. *J. Environ. Manage.* 147. <https://doi.org/10.1016/j.jenvman.2014.09.005>
- 803 Liu, Y., Wang, C., Yu, Y., Chen, Y., Du, L., Qu, X., Peng, W., Zhang, M., Gui, C., 2019. Effect of urban stormwater road  
804 runoff of different land use types on an urban river in Shenzhen, China. *Water (Switzerland)* 11.  
805 <https://doi.org/10.3390/w11122545>
- 806 Loperfido, J. V., Noe, G.B., Jarnagin, S.T., Hogan, D.M., 2014. Effects of distributed and centralized stormwater best  
807 management practices and land cover on urban stream hydrology at the catchment scale. *J. Hydrol.* 519.  
808 <https://doi.org/10.1016/j.jhydrol.2014.07.007>
- 809 Ludwig, J., Sanbonmatsu, L., Gennetian, L., Adam, E., Duncan, G.J., Katz, L.F., Kessler, R.C., Kling, J.R., Lindau, S.T.,  
810 Whitaker, R.C., McDade, T.W., 2011. Neighborhoods, Obesity, and Diabetes — A Randomized Social Experiment. *N.*  
811 *Engl. J. Med.* 365. <https://doi.org/10.1056/nejmsa1103216>
- 812 Maas, J., van Dillen, S.M.E., Verheij, R.A., Groenewegen, P.P., 2009. Social contacts as a possible mechanism behind the  
813 relation between green space and health. *Heal. Place* 15. <https://doi.org/10.1016/j.healthplace.2008.09.006>
- 814 Madureira, H., Andresen, T., 2014. Planning for multifunctional urban green infrastructures: Promises and challenges. *Urban*  
815 *Des. Int.* 19. <https://doi.org/10.1057/udi.2013.11>
- 816 Marchese, D., Reynolds, E., Bates, M.E., Morgan, H., Clark, S.S., Linkov, I., 2018. Resilience and sustainability: Similarities and  
817 differences in environmental management applications. *Sci. Total Environ.* <https://doi.org/10.1016/j.scitotenv.2017.09.086>
- 818 Martikainen, P., Mäki, N., Blomgren, J., 2004. The effects of area and individual social characteristics on suicide risk: A  
819 multilevel study of relative contribution and effect modification. *Eur. J. Popul.* 20. <https://doi.org/10.1007/s10680-004-3807-1>
- 820
- 821 Mitchell, R., Popham, F., 2008. Effect of exposure to natural environment on health inequalities: an observational population  
822 study. *Lancet* 372. [https://doi.org/10.1016/S0140-6736\(08\)61689-X](https://doi.org/10.1016/S0140-6736(08)61689-X)
- 823 Nkoy, F.L., Stone, B.L., Knighton, A.J., Fassl, B.A., Johnson, J.M., Maloney, C.G., Savitz, L.A., 2018. Neighborhood  
824 Deprivation and Childhood Asthma Outcomes, Accounting for Insurance Coverage. *Hosp. Pediatr.* 8.  
825 <https://doi.org/10.1542/hpeds.2017-0032>
- 826 Pande, S., Sivapalan, M., 2017. Progress in socio-hydrology: a meta-analysis of challenges and opportunities. *Wiley Interdiscip.*  
827 *Rev. Water* 4. <https://doi.org/10.1002/wat2.1193>
- 828 Perez-Pedini, C., Limbrunner, J.F., Vogel, R.M., 2005. Optimal Location of Infiltration-Based Best Management Practices for  
829 Storm Water Management. *J. Water Resour. Plan. Manag.* 131. [https://doi.org/10.1061/\(asce\)0733-9496\(2005\)131:6\(441\)](https://doi.org/10.1061/(asce)0733-9496(2005)131:6(441))
- 830 Perica, S., Pavlovic, S., Laurent, M. St., Trypaluk, C., Unruh, D., Wilhite, O., 2018. NOAA Atlas 14 Precipitation-Frequency  
831 Atlas of the United States Volume 11 Version 2.0: Texas.
- 832 Pitt, R., Maestre, A., Clary, J., 2015. National Stormwater Quality Database (NSQD), Version 4.02 (2001-2015).
- 833 Ray, H., Jakubec, S.L., 2014. Nature-based experiences and health of cancer survivors. *Complement. Ther. Clin. Pract.* 20.  
834 <https://doi.org/10.1016/j.ctcp.2014.07.005>
- 835 Rossi, L., Fankhauser, R., Chèvre, N., 2006. Water quality criteria for total suspended solids (TSS) in urban wet-weather  
836 discharges. *Water Sci. Technol.* 54. <https://doi.org/10.2166/wst.2006.623>
- 837 Rossman, L., 2014. National Stormwater Calculator User's Guide: Version 1.1.
- 838 Rossman, L.A., Huber, W.C., 2016. Storm Water Management Model User's Manual, United States Environment Protection  
839 Agency.
- 840 Ruangpan, L., Vojinovic, Z., Di Sabatino, S., Leo, L.S., Capobianco, V., Oen, A.M.P., McClain, M.E., Lopez-Gunn, E., 2020.  
841 Nature-based solutions for hydro-meteorological risk reduction: a state-of-the-art review of the research area. *Nat. Hazards*  
842 *Earth Syst. Sci.* 20. <https://doi.org/10.5194/nhess-20-243-2020>
- 843 Saboohi, Y., 2001. An evaluation of the impact of reducing energy subsidies on living expenses of households. *Energy Policy* 29.  
844 [https://doi.org/10.1016/S0301-4215\(00\)00116-6](https://doi.org/10.1016/S0301-4215(00)00116-6)
- 845 Sadras, V., Bongiovanni, R., 2004. Use of Lorenz curves and Gini coefficients to assess yield inequality within paddocks. *F.*  
846 *Crop. Res.* 90. <https://doi.org/10.1016/j.fcr.2004.04.003>
- 847 Sarabi, S., Han, Q., Romme, A.G.L., de Vries, B., Valkenburg, R., den Ouden, E., 2020. Uptake and implementation of Nature-  
848 Based Solutions: An analysis of barriers using Interpretive Structural Modeling. *J. Environ. Manage.* 270.  
849 <https://doi.org/10.1016/j.jenvman.2020.110749>
- 850 Sarabi, S.E., Han, Q., Romme, A.G.L., de Vries, B., Wendling, L., 2019. Key enablers of and barriers to the uptake and  
851 implementation of nature-based solutions in urban settings: A review. *Resources.*  
852 <https://doi.org/10.3390/resources8030121>

Non-peer reviewed EarthArXiv preprint.  
Under review by *Journal of Hydrology*

- 853 Sarma, P.B.S., Delleur, J.W., Rao, A.R., 1973. Comparison of rainfall-runoff models for urban areas. *J. Hydrol.* 18.  
854 [https://doi.org/10.1016/0022-1694\(73\)90056-5](https://doi.org/10.1016/0022-1694(73)90056-5)
- 855 Schlossberg, M., 2003. GIS, the US census and neighbourhood scale analysis. *Plan. Pract. Res.* 18.  
856 <https://doi.org/10.1080/0269745032000168269>
- 857 SFEI, 2020. GreenPlan-IT Case Study: San Jose's Urban Villages, Chapter 3.
- 858 SFEI, 2018. GreenPlanIT Optimization Tool User Manual.
- 859 Singh, G.K., 2003. Area Deprivation and Widening Inequalities in US Mortality, 1969-1998. *Am. J. Public Health* 93.  
860 <https://doi.org/10.2105/AJPH.93.7.1137>
- 861 Sun, T., Zhang, H., Wang, Y., Meng, X., Wang, C., 2010. The application of environmental Gini coefficient (EGC) in allocating  
862 wastewater discharge permit: The case study of watershed total mass control in Tianjin, China. *Resour. Conserv. Recycl.*  
863 54. <https://doi.org/10.1016/j.resconrec.2009.10.017>
- 864 TNRIS, 2019. Harris County LiDAR 2018.
- 865 University of Wisconsin School of Medicine and Public, 2019. Area Deprivation Index.
- 866 USDA, 1986. Urban Hydrology for Small Watersheds: TR-55.
- 867 USGS, 2021a. USGS 08074020 Whiteoak Bayou at Alabonson Rd, Houston, TX.
- 868 USGS, 2021b. USGS 08074500 Whiteoak Bayou at Houston, TX.
- 869 Van de Meene, S.J., Brown, R.R., Farrelly, M.A., 2011. Towards understanding governance for sustainable urban water  
870 management. *Glob. Environ. Chang.* 21. <https://doi.org/10.1016/j.gloenvcha.2011.04.003>
- 871 van den Bosch, M., Ode Sang, 2017. Urban natural environments as nature-based solutions for improved public health – A  
872 systematic review of reviews. *Environ. Res.* 158. <https://doi.org/10.1016/j.envres.2017.05.040>
- 873 Wamsler, C., Wickenberg, B., Hanson, H., Alkan Olsson, J., Stålhammar, S., Björn, H., Falck, H., Gerell, D., Oskarsson, T.,  
874 Simonsson, E., Torffvit, F., Zelmerlow, F., 2020. Environmental and climate policy integration: Targeted strategies for  
875 overcoming barriers to nature-based solutions and climate change adaptation. *J. Clean. Prod.* 247.  
876 <https://doi.org/10.1016/j.jclepro.2019.119154>
- 877 White, M., Harmel, D., Yen, H., Arnold, J., Gambone, M., Haney, R., 2015. Development of Sediment and Nutrient Export  
878 Coefficients for U.S. Ecoregions. *J. Am. Water Resour. Assoc.* 51. <https://doi.org/10.1111/jawr.12270>
- 879 White, T.J., 2007. Sharing resources: The global distribution of the Ecological Footprint. *Ecol. Econ.* 64.  
880 <https://doi.org/10.1016/j.ecolecon.2007.07.024>
- 881 Wihlborg, M., Sörensen, J., Alkan Olsson, J., 2019. Assessment of barriers and drivers for implementation of blue-green  
882 solutions in Swedish municipalities. *J. Environ. Manage.* 233. <https://doi.org/10.1016/j.jenvman.2018.12.018>
- 883 Wu, J., Kauhanen, P.G., Hunt, J.A., Senn, D.B., Hale, T., McKee, L.J., 2019. Optimal Selection and Placement of Green  
884 Infrastructure in Urban Watersheds for PCB Control. *J. Sustain. Water Built Environ.* 5.  
885 <https://doi.org/10.1061/jswbay.0000876>
- 886 Yan, D., Jia, Z., Xue, J., Sun, H., Gui, D., Liu, Y., Zeng, X., 2018. Inter-regional coordination to improve equality in the  
887 agricultural virtualwater trade. *Sustain.* 10. <https://doi.org/10.3390/su10124561>
- 888 Yang, L., Jin, S., Danielson, P., Homer, C., Gass, L., Bender, S.M., Case, A., Costello, C., Dewitz, J., Fry, J., Funk, M.,  
889 Granneman, B., Liknes, G.C., Rigge, M., Xian, G., 2018. A new generation of the United States National Land Cover  
890 Database: Requirements, research priorities, design, and implementation strategies. *ISPRS J. Photogramm. Remote Sens.*  
891 146. <https://doi.org/10.1016/j.isprsjprs.2018.09.006>
- 892 Zhang, D., Shen, J., Liu, P., Zhang, Q., Sun, F., 2020. Use of fuzzy analytic hierarchy process and environmental gini coefficient  
893 for allocation of regional flood drainage rights. *Int. J. Environ. Res. Public Health* 17.  
894 <https://doi.org/10.3390/ijerph17062063>
- 895 Zhang, K., Chui, T.F.M., 2018. A comprehensive review of spatial allocation of LID-BMP-GI practices: Strategies and  
896 optimization tools. *Sci. Total Environ.* <https://doi.org/10.1016/j.scitotenv.2017.11.281>
- 897
- 898



899  
900  
901  
902  
903

## SUPPLEMENTARY MATERIAL

### Optimal planning of natural stormwater solutions using a composite Gini coefficient: A watershed assessment of hydrological, environmental, social, and economic efficiency

*Cyndi V. Castro*

904  
905  
906  
907  
908  
909  
910  
911  
912  
913  
914  
915  
916  
917  
918

#### Contents of this file:

Supplementary Tables

- Table S.1 Case study rainfall coefficients.
- Table S.2 Pollutant load parameters.
- Table S.3 PCSWMM water balance zones.
- Table S.4 PCSWMM parameter inputs.
- Table S.5 Integrated square error for model calibration.
- Table S.6 Integrated square error for model validation.
- Table S.7 GreenPlan-IT optimization input parameters.

Supplementary Figures

- Fig. S.1 PCSWMM storm events.
- Fig. S.2 Model sensitivity analysis.
- Fig. S.3 Model calibration output hydrographs.

**Table S.1.** Atlas 14 rainfall coefficients for Houston, Texas, USA.

Rainfall Frequency	<b>b</b> (inches)	<b>d</b> (minutes)	<b>e</b>
2-Year (50% AEP)	47.25	8.94	0.7263
5-Year (20% AEP)	54.09	8.34	0.7051
10-Year (10% AEP)	55.26	7.30	0.6752
25-Year (4% AEP)	56.72	6.12	0.6397
50-Year (2% AEP)	57.94	5.47	0.6166
100-Year (1% AEP)	56.68	4.46	0.5857

**Table S.2.** Pollutant load parameters for modeling total suspended solids (TSS).

Land Use	TSS (mg/L)	Removal Efficiency (%)		
		<i>Porous Pavement</i>	<i>Bioretention Cell</i>	<i>Tree Box</i>
Industrial	145.43			
Residential	146.00			
Mixed Use	72.93	60%	50%	50%
Commercial	92.56			
Open Space	211.33			

920 **Table S.3.** Water balance zones represented in the WOB case study.

<b>NBS Feature</b>	<b>Surface</b>	<b>Soil</b>	<b>Storage</b>	<b>Underdrain</b>
Porous Pavement	X		X	X
Bioretention Cell	X	X	X	X
Tree Box	X	X	X	

921

922 **Table S.4.** PCSWMM LID Control Editor parameter inputs. BIOR: “Bioretention cell”, PMPV:  
923 “Permeable pavement”, TRBX: “Tree box”.

	<b>Parameter</b>	<b>NBS Feature</b>			<b>Units</b>
		<b>BIOR</b>	<b>PMPV</b>	<b>TRBX</b>	
Surface	Berm height	9	0	12	Inch
	Vegetation volume	0	0	0.2	Fraction
	Surface roughness	0.1	0.1	0.1	-
	Surface slope	1.0	1.0	1.0	Percent
Pavement	Thickness	-	4	-	Inch
	Void ratio	-	0.15	-	Voids/solids
	Impervious surface	-	0	-	Fraction
	Permeability	-	100	-	Inch/hour
Soil	Thickness	18	0	21	Inch
	Porosity	0.5	0.5	0.5	Volume fraction
	Field capacity	0.2	0.2	0.2	Volume fraction
	Wilting point	0.1	0.1	0.1	Volume fraction
	Conductivity	5	0.5	50	Inch/hour
	Conductivity slope	10	10	10	-
	Suction head	3.5	3.5	3.5	Inch
	Thickness	12	24	6	Inch
Storage	Void ratio	0.75	0.75	0.75	Voids/solids
	Seepage rate	0.5	5	0.5	Inch/hour
	Clogging factor	0	0	0	-
	Drain coefficient	5	100	50	Inch/hour
Drain	Drain exponent	0.5	0.5	0.5	-
	Drain offset height	12	8	0	Inch

924

925 **Table S.5.** ISE statistics between simulated and observed flows for calibration.

Storm Event No.	Date	Gauge No. 08074500	Gauge No. 08074020
		Rating (ISE)	
1	Nov. 27, 2020	Good (8.4)	Good (6.3)
2	Dec. 2, 2020	Good (8.9)	Good (10.0)
3	Dec. 11, 2020	Good (9.3)	Fair (11.3)
4	Dec. 13, 2020	Fair (13.7)	Good (6.3)
5	Dec. 19, 2020	Very Good (5.9)	Good (8.3)
6	Dec. 30, 2020	Good (10.0)	Very Good (6.0)
7	Jan. 6, 2021	Good (10.7)	Fair (11.0)
8	Jan. 10, 2021	Good (7.2)	Good (7.5)
9	Feb. 11, 2021	Good (8.3)	Good (7.5)
10	Feb. 17, 2021	Very Good (4.6)	Good (7.1)

926

927 **Table S.6.** ISE statistics between simulated and observed flows for validation.

Storm Event No.	Date	Gauge No. 08074500	Gauge No. 08074020
		Rating (ISE)	
1	Apr. 30, 2021	Very Good (4.7)	Very Good (5.9)
2	May 16, 2021	Very Good (5.9)	Very Good (5.9)
3	May 22, 2021	Very Good (4.8)	Very Good (4.9)
4	Jun. 2, 2021	Good (6.8)	Good (7.6)
5	Jun. 27, 2021	Good (8.8)	Very Good (4.6)
6	Jul. 3, 2021	Very Good (4.5)	Very Good (4.9)
7	Jul. 8, 2021	Very Good (5.2)	Good (9.0)
8	Jul. 15, 2021	Very Good (5.6)	Good (6.4)

928

929

930

931

932 **Table S.7.** GreenPlan-IT Optimization Tool subcatchment input file. BIOR: “Bioretention cell”,  
933 PMPV: “Permeable pavement”, TRBX: “Tree box”.

Subcatchment No.	Area (AC)	Impervious Cover (%)	No. Possible NBS Features		
			BIOR	PMPV	TRBX
1	709.4	43.7	4904	96	7761
2	1420.5	45.4	18158	317	17632
3	683	40.7	8178	37	10573
4	363.1	47.6	1449	43	9745
5	588.5	33.5	6639	229	214
6	358.6	51.5	1815	4	9404
7	712	32.5	17376	93	3208
8	815	46.5	12339	362	4034
9	913	43.7	11430	157	14351
10	432.8	40.9	4932	96	387
11	584.9	52	4521	133	9299
12	62.4	32.6	1385	4	22
13	86.7	47.8	937	0	1984
14	1018.4	34.8	7250	192	11130
15	519.2	50.7	6103	194	8295
16	358.4	33.9	4273	38	3359
17	270.7	54.7	1537	35	8309
18	256.3	59	680	17	10540
19	871.2	59	6796	333	12400
20	300.7	24.7	1780	123	259
21	197.7	59.1	1602	195	231
22	399.5	64.3	3392	313	5719
23	519	31.4	8859	55	0
24	382.5	42.9	3635	183	547
25	226.8	52.6	1843	18	3654
26	447.7	41.8	6841	87	643
27	502.9	59.5	5273	217	7760
28	358.4	39.2	3186	143	168
29	282.3	20.1	4122	10	0
30	614.4	41.7	6045	7	4934
31	42.5	65.9	284	69	154
32	153.3	31.6	3360	0	1519
33	340.4	51.1	6349	341	131
34	83.4	62.3	1074	63	145
35	261.7	44	1175	7	488

**Table S.7** (continued):

Subcatchment No.	Area (AC)	Impervious Cover (%)	No. Possible NBS Features		
			BIOR	PMPV	TRBX
36	458.3	54.5	3629	44	11804
37	966.4	51.6	12159	287	9376
38	279.7	43.4	1746	87	968
39	1004	37.3	5286	31	1553
40	47	28.4	1330	0	105
41	480.7	43.8	6856	215	857
42	169.6	38.6	2098	0	4163
43	391	31.5	1486	13	1441
44	341.4	51.6	5228	174	157
45	413.6	43.5	4583	31	1472
46	69.5	18.6	1041	0	339
47	467.3	49.7	4184	311	302
48	1197.9	51.8	11504	399	16692
49	590.3	52.2	4907	96	14166
50	250.2	53.9	1181	88	6201
51	562	41.4	5508	23	12750
52	549.5	42.9	4888	28	11791
53	312.8	57.8	1122	14	10247
54	333.8	38.6	5519	51	884
55	108.4	39.6	1592	77	0
56	431.6	41.5	4998	8	8551
57	349.6	22.6	3603	30	1829
58	712.5	43.2	5598	60	11214
59	96.6	37.1	1051	0	2461
60	35.2	54.9	443	0	64
61	358.6	37.3	3386	24	6237
62	318.4	63.7	3010	343	866
63	61.4	42.8	352	0	909
64	302.1	42.1	1288	32	2621
65	811.4	47.7	6421	248	6760
66	182.1	49.6	2088	121	2277
67	0.7	13.8	25	0	0
68	326.9	49.4	1317	29	3681
69	1903.1	55.1	13296	1533	18592
70	171.7	61.5	1461	135	1313
71	1017	29.8	21837	97	6886

**Table S.7** (continued):

<b>Subcatchment No.</b>	<b>Area (AC)</b>	<b>Impervious Cover (%)</b>	<b>No. Possible NBS Features</b>		
			<b>BIOR</b>	<b>PMPV</b>	<b>TRBX</b>
73	501.5	39.8	6885	29	3604
74	909.5	55.3	13125	525	3490
75	237.6	73	1157	241	52
76	596.7	51.5	8741	299	2639
77	275.4	40.3	2623	12	3336
78	1023.3	52.4	8928	816	9392
79	404.2	59.7	3704	442	3597
80	93.8	48.5	542	36	376
81	163.5	73.3	534	164	1366
82	1398	62.6	6316	1408	15463
83	314.7	55.6	3722	141	1979
84	123.5	34.2	1365	4	828
85	551.8	49.5	4846	335	2798
86	388.8	32.5	5615	7	2605
87	564.6	40	6756	103	2275
88	1.2	58.9	14	0	11
89	1190.6	55.6	7910	463	18147
90	489.7	65.1	3051	472	4521
91	634.5	40.4	5931	143	2033
92	293.6	54.7	3685	215	233
93	814.7	67.1	3245	915	6251
94	407.7	38.4	6199	48	5144
95	448.8	59.3	2304	301	2699
96	484.7	35.2	11246	123	2632
97	142.4	43.8	1735	27	915
98	317.7	47.5	2468	87	6240
99	488.3	62.1	4068	354	5290
100	219.5	48.7	1717	80	2722
101	375.6	61	4213	207	2548
102	627.4	47.2	3638	141	8215
103	185.9	44.6	1712	23	2889
105	103.5	54.8	913	61	701
106	90.2	59	339	19	1367
107	604.3	51	2368	221	12431
108	947.3	55	5377	183	18362
109	589.4	46.3	2149	195	6186

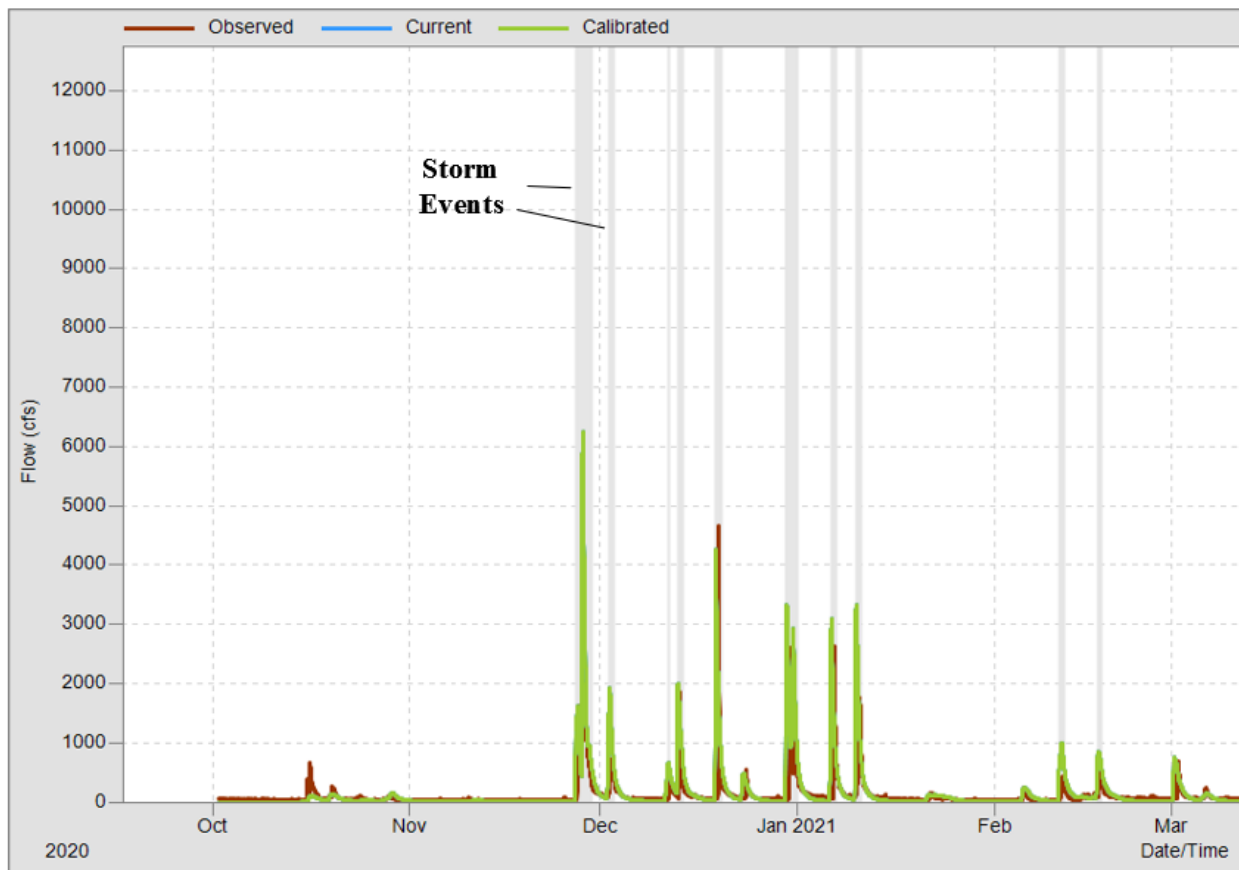
**Table S.7** (continued):

Subcatchment No.	Area (AC)	Impervious Cover (%)	No. Possible NBS Features		
			BIOR	PMPV	TRBX
111	339.2	68.4	1326	371	2715
112	236.7	61.1	621	115	7151
113	45.8	72.1	72	68	339
114	518.8	53.8	2244	150	12494
116	278.7	47.1	1650	42	3050
117	11.1	44.5	18	0	26
118	350.3	55.5	1165	186	4659
119	413.9	38.5	6706	26	4730
120	150.9	64.9	572	207	2181
121	264.1	43.1	1289	101	1848
123	144.6	56	528	98	984
124	383.9	56.2	2068	186	3162
125	252.5	60.8	637	141	4223
126	10.6	47.9	7	0	0
127	24.6	72.9	50	52	57
128	489	48.5	1604	91	2793
129	258	59	403	159	2750
130	367.1	58.1	1306	232	2556
131	6.4	53.2	11	0	119
132	284.7	60.3	765	233	3487
133	314.7	60.6	532	155	3444
134	296.5	63.3	1974	206	1981
135	484.7	51.3	1866	255	4755
136	335.2	80.9	486	687	3635
137	1051.4	63.4	2509	880	16024
138	753.6	56.7	2267	471	10215
139	448.8	80.6	617	921	3912
140	721.4	57.3	2162	329	11066
141	291.7	59.4	1007	126	2480
143	263.4	64.1	824	212	4076
144	747.2	68.3	345	698	23024
145	725.4	60.9	1298	395	15412
146	247.3	47.2	1255	23	5297
147	38.5	43	307	6	478
148	411.3	65.1	81	110	16841
149	147.6	68.7	107	96	4682

**Table S.7** (continued):

Subcatchment No.	Area (AC)	Impervious Cover (%)	No. Possible NBS Features		
			BIOR	PMPV	TRBX
151	392.6	65.1	154	61	17508
152	379.4	55.9	916	171	9809
153	10.9	33.6	114	0	225
154	540.7	68.2	1114	314	10807
155	820.9	64.3	3071	998	12983
156	593.4	60.4	223	37	23936
157	94.3	56.3	596	13	2427
158	218	56.1	874	23	8214
159	177.2	55.1	982	62	4267
160	660.5	64.6	2867	750	13880
161	483.1	69	1038	559	8147
162	486.4	70.5	590	395	11047

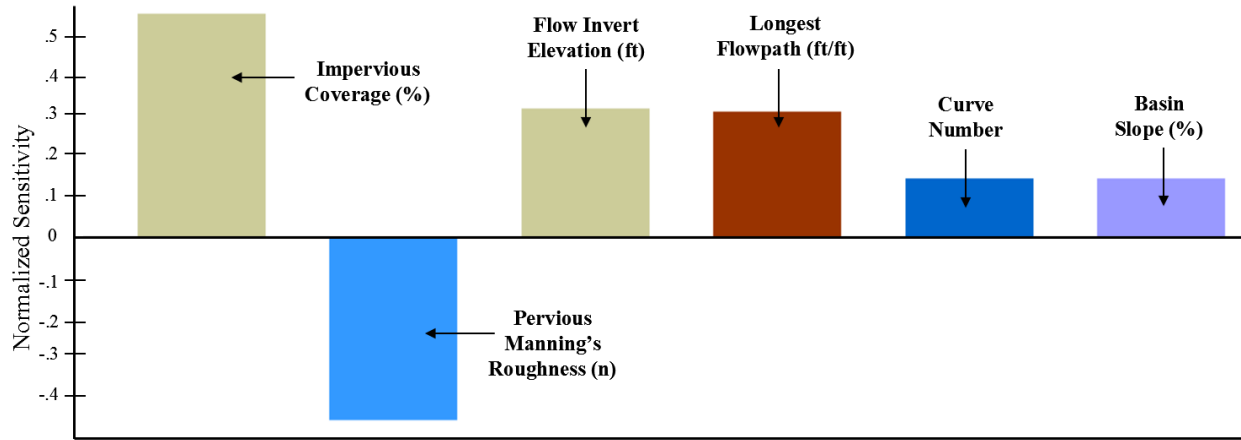
938



939

940 **Fig. S.1.** Sample of storm event selection in PCSWMM.

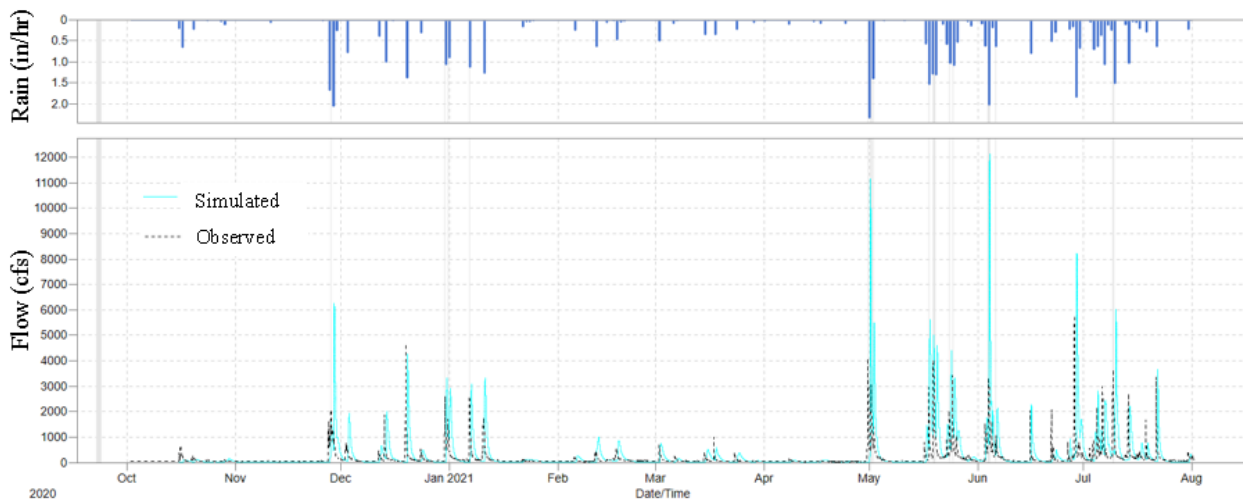




941

942 **Fig. S.2.** Normalized sensitivity analysis output for primary variables.

943



944

945 **Fig. S.3.** Calibration output hydrographs for USGS Gauge No. 08074500.